Journal of Cardiovascular Pharmacology™
42 (Suppl. 1):S7–S10 © 2003 Lippincott Williams & Wilkins, London

Acute Limb Ischemia does not Facilitate but Inhibits Norepinephrine Release from Muscle Sympathetic Nerve Endings in Anesthetized Rabbit

Noriyuki Tokunaga, Toji Yamazaki, Tsuyoshi Akiyama, *Shunji Sano and Hidezo Mori

*Department of Cardiac Physiology, National Cardiovascular Center Research Institute, Osaka, Japan; *Department of Cardiovascular Surgery, Okayama University Medical School, Okayama, Japan*

Summary: Although myocardial ischemia is associated with regional cardiac sympathetic nerve deterioration, it remains unknown whether acute hindlimb ischemia impairs muscle sympathetic nerve function. In the study presented here we implanted dialysis probes in the adductor muscle of anesthetized rabbits and measured dialysate norepinephrine levels as an index of muscle sympathetic nerve activity. Acute hindlimb ischemia was induced by injection of microspheres and occlusion of the common iliac artery. Dialysate norepinephrine levels decreased from 19.3 ± 3.5 pg/ml at control to 9.4 ± 3.7 pg/ml at 30 min of ischemia and further to 1.7 ± 0.2 pg/ml at 75 min of ischemia. During acute hindlimb ischemia, baroreflex (bilateral carotid occlusion) and high potassium level-induced norepinephrine response was inhibited, but tyramine-induced norepinephrine response was preserved. In conclusion, acute hindlimb ischemia caused decreases in dialysate norepinephrine levels. This reduction may be mediated by an impairment of axonal conduction and/or of norepinephrine releasing function at skeletal muscle sympathetic nerve endings. **Key Words:** Acute limb ischemia—Muscle sympathetic nerve—Norepinephrine release.

INTRODUCTION

Acute occlusion of an artery supplying an organ reduces blood flow, decreases tissue pO_2 and increases tissue pCO_2, leading to anaerobic glucose metabolism (1), increment in lactate production (2), acidosis and depletion of high-energy phosphate (2). Such tissue ischemia is accompanied by deterioration of the innervated sympathetic tract. It is known, for example, that myocardial ischemia affects the sympathetic nerve pathway at axonal and nerve endings (3,4). However, little information is available on the skeletal muscle sympathetic nerve.

Sympathetic nerve innervation in skeletal muscle is evident from histochemical and electrophysiological studies (5,6). A number of studies on skeletal muscle sympathetic nerve activities have been reported (6,7). However, nerve recordings do not provide information about sympathetic nerve ending function. Data on norepinephrine (NE) spillover suggested that as much as 20–30% of the NE entering the circulation derives from skeletal muscle sympathetic nerve endings (8). Thus, small increments in NE release at the skeletal muscle sympathetic nerve may affect circulating plasma NE levels and systemic hemodynamics.

Recently, we reported that using a microdialysis technique with high performance liquid chromatography is a sensitive and versatile method for monitoring interstitial NE levels in the myocardial ischemic region (9). In the study presented here, we applied the microdialysis technique to the skeletal muscle of anesthetized rabbits. Using this method, we investigated how acute limb ischemia affects NE release from skeletal muscle sympathetic nerve endings.

METHODS

Animal preparation

Male Japanese white rabbits, each weighing 2.6–3.1 kg, were anesthetized with pentobarbital sodium (30–35 mg/kg, i.v.). The level of anesthesia was maintained with a continuous intravenous infusion of pentobarbital sodium (1–2 mg/kg per h). After tracheostomy, the animals were ventilated with room air mixed with oxygen. Body temperature was maintained with a heated pad and lamp. All protocols were performed in accor-

Address correspondence and requests for reprints to Toji Yamazaki, Department of Cardiac Physiology, National Cardiovascular Center Research Institute, 5-7-1 Fujishiro-dai, Suita, Osaka 565-8565, Japan. E-mail: yamazaki@ri.ncvc.go.jp

dance with the American Physiological Society guidelines for the use of animals. An electrocardiogram, heart rate and arterial blood pressure were simultaneously monitored with a data recorder. After a longitudinal skin incision was made in the left groin, the dialysis probes were implanted in the left adductor muscle with a fine guiding needle.

Dialysis technique and NE measurements

Using the dialysis technique, dialysate NE concentrations were measured as an index of skeletal muscle interstitial NE levels. For skeletal muscle dialysis, we designed a transverse dialysis probe. The dialysis fiber [13 mm length, 0.31 mm outside diameter (OD) and 0.2 mm inside diameter (ID); PAN-1200, 50 000 molecular mass cut-off, Asahi Chemical, Tokyo, Japan] was glued at both ends into a polyethylene tube (25 cm length, 0.5 mm OD and 0.2 mm ID) (10). The dialysis probe was perfused with Ringer solution at a speed of 10 μl/min using a microinjection pump (CMA 102; Carnergie Medicin, Stockholm, Sweden). In the preliminary experiment we examined the time course of dialysate NE concentrations after the probe implantation. Dialysate NE concentrations reached an almost steady level at 120 min after probe implantation. Therefore in the experimental protocol dialysate sampling was started 120 min after probe implantation.

Dialysate NE concentrations were measured by high performance liquid chromatography with electrochemical detection (ECD-300; Eicom, Kyoto, Japan) after removing interfering compounds in the dialysate by an alumina procedure (11).

Experimental protocols

Acute limb ischemia was induced by injection of nonradioactive iodine-labeled microspheres (15 μm in diameter, 1×10^8/kg; Sekisui Plastic, Osaka, Japan) through the left common iliac artery, as previously described (12). After the injection, the common iliac artery was ligated.

Protocol 1: Time course of dialysate NE during acute limb ischemia

In order to examine the time course of dialysate NE concentrations during acute ischemia, we measured dialysate NE concentrations over a period of 75 min of ischemia in six rabbits. The sampling period for collecting dialysate was 15 min (one dialysate sample volume = 150 μl).

Protocol 2: Influence of acute limb ischemia on dialysate NE response evoked by bilateral carotid occlusion

In order to examine the influence of acute limb ischemia on central mediated baroreflex-induced NE releasing function, we performed bilateral carotid occlusion (BCO) in six rabbits. After transection of aortic nerves, the common carotid arteries were occluded with bulldog clamps for 2.5 min. In order to collect sufficient NE during a defined time period, we decided to implant two dialysis probes > 5 mm apart and the dialysate samples were collected from them simultaneously. Dialysates were pooled as one sample. Bilateral carotid occlusion responses were repeated at control and after 75 min of ischemia.

Protocol 3: Influence of acute limb ischemia on tyramine-induced and high potassium-induced dialysate NE response

The influence of acute limb ischemia on the regional sympathetic nerve function was examined by local administration of NE-releasing agents through the dialysis probe. Tyramine (NE-releasing sympathomimetic amine, 600 μM)-induced NE efflux closely reflects the NE content at the nerve endings (13). Tyramine-induced dialysate NE responses were measured at control and after 75 min of ischemia in separate rabbits. High potassium-induced NE response was caused by exocytotic NE release from sympathetic nerve endings. We administered high potassium levels (KCl, 100 mM) locally through the dialysis probe, and the dialysate NE response was obtained at control and after 75 min of ischemia.

Statistical analysis

Statistical analysis of the multiple comparison was performed by analysis of variance followed by Fisher's parametric least significant difference test. Student's *t*-tests were used for the comparison of the two variables. Statistical significance was defined as $p < 0.05$. Values are presented as mean ± SE.

RESULTS

Hemodynamic variables of arterial pressure and heart rate were unaltered before and during ischemia. Further local administration of tyramine and KCl did not affect hemodynamic variables.

Protocol 1: Time course of dialysate NE during acute limb ischemia

Figure 1 shows the time course of the dialysate NE concentrations before and during ischemia. Acute ischemia decreased the dialysate NE concentrations from 19.3 ± 3.5 pg/ml at control to 9.4 ± 3.7 pg/ml at 30 min of ischemia. The dialysate NE concentrations continued to decline progressively, and reached 1.7 ± 0.2 pg/ml at 75 min of ischemia.

Protocol 2: Influence of acute limb ischemia on dialysate NE response evoked by BCO

There were no significant differences in the mean arterial pressure response to BCO between control and ischemia (59.7 ± 3.5 and 62.0 ± 3.0 mmHg). Figure 2 shows the response of dialysate NE concentrations to BCO at control and after ischemia. At control, BCO increased dialysate NE concentrations from 19.6 ± 4.7 pg/ml to 34.5 ± 9.2 pg/ml. At 75 min of ischemia, BCO did not increase dialysate NE concentrations. The BCO-induced increment in dialysate NE was attenuated at 75 min of ischemia.

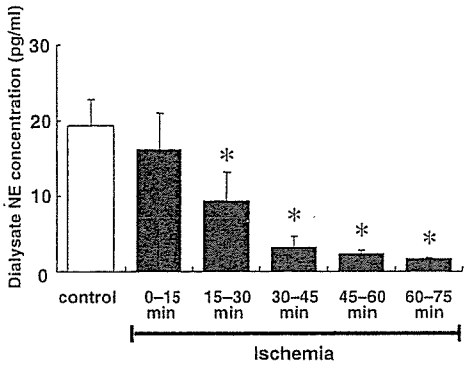

FIG. 1. Time course of the dialysate norepinephrine (NE) concentrations during acute limb ischemia (n = 6). Acute limb ischemia progressively decreased dialysate NE concentration. Data are mean ± SE. *p < 0.05 versus control.

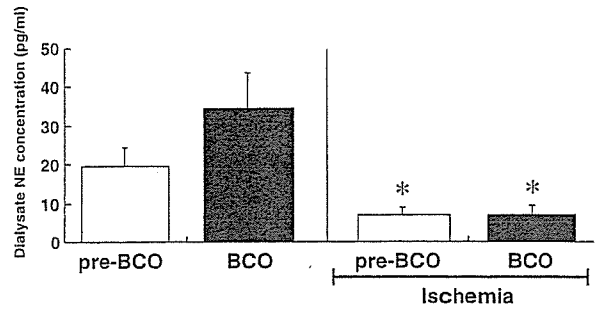

FIG. 2. The responses of dialysate norepinephrine (NE) concentration to bilateral carotid occlusion (BCO) (n = 6). At control, BCO significantly increased dialysate NE concentrations, whereas after 75 min of ischemia, BCO did not alter dialysate NE concentrations. Data are mean ± SE. *p < 0.05 versus control.

Protocol 3: Influence of acute limb ischemia on tyramine-induced and high potassium-induced dialysate NE responses

Local administration of KCl was performed at control and 75 min of ischemia in separate rabbits. Figure 3 shows KCl-induced dialysate NE concentrations. At control, KCl increased the dialysate NE concentrations from 11.7 ± 2.8 pg/ml at baseline to 84.7 ± 20.8 pg/ml. At 75 min of ischemia, KCl increased the dialysate NE concentrations from 1.8 ± 1.1 pg/ml at baseline to 35.0 ± 10.3 pg/ml. This KCl-induced increment in dialysate NE was attenuated at 75 min of ischemia. Local administration of tyramine was performed at control and after 75 min of ischemia in separate rabbits. At control, tyramine increased the dialysate NE concentrations from 15.4 ± 2.4 pg/ml at baseline to 106.0 ± 20.4 pg/ml. At 75 min of ischemia, tyramine also increased the dialysate NE concentrations from 3.8 ± 1.1 pg/ml at baseline to 151.0 ± 23.0 pg/ml (n = 8). This increment did not differ between control and ischemia.

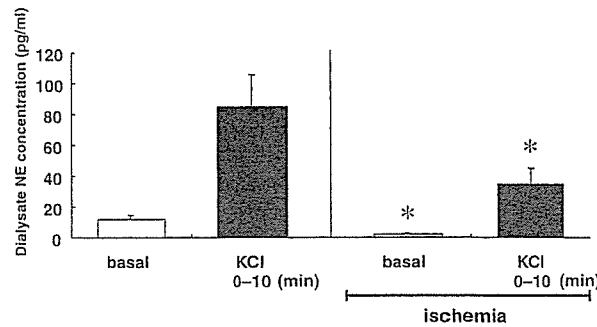

FIG. 3. The responses of dialysate norepinephrine (NE) concentration to locally applied KCl (100 mM). At control (n = 5), KCl significantly increased dialysate NE concentrations, whereas after 75 min of ischemia (n = 6), KCl attenuated dialysate NE response. Data are mean ± SE. *p < 0.05 versus control.

DISCUSSION

In this study, we have demonstrated that: (i) acute limb ischemia progressively decreased dialysate NE concentrations; (ii) dialysate NE response to BCO was diminished in acute limb ischemia; and (iii) dialysate NE response to local administration of KCl became blunted in acute limb ischemia.

Two types of experimental ischemia model were proposed in the skeletal muscle: post-exercise muscle ischemia and flow reduction by microspheres and/or occlusion (12,14). During post-handgrip muscle ischemia, mean arterial pressure and muscle sympathetic nerve activities were elevated. This perturbation was used as a mild, temporary and reversible ischemic model. Compared with myocardial ischemia, a severe and irreversible ischemic model was chosen to induce skeletal muscle ischemia in this study (14). During the ischemia, mean arterial pressure and heart rate were not altered. To our knowledge, this is the first report covering the influence of acute limb ischemia on skeletal muscle dialysate NE levels. During the period of ischemia, dialysate NE concentrations continued to decline progressively and had decreased one-tenth by the end of the period of ischemia. The levels of skeletal muscle interstitial NE are altered by circulating plasma NE and surrounding sympathetic nerve activity (12). Local administration of tetrodotoxin (Na^+ channel blocker, 10 μM) markedly decreased the skeletal muscle dialysate NE. This result suggested that one-third of dialysate NE is derived from circulating NE under resting conditions. Therefore, the overall reduction of dialysate NE cannot be explained by reduction in the extraction from circulating NE.

Bilateral carotid occlusion induced increases in heart rate, mean arterial pressure and dialysate NE levels. During the ischemia, heart rate and arterial pressure responses were preserved but dialysate NE response was blunted. These results indicate that the systemic response to BCO was intact, while the skeletal muscle sympathetic response was impaired in ischemic regions. Earlier studies reported that acute limb ischemia reduced the con-

duction of motor nerves such as the sciatic nerve (16), and induced axonal degeneration histologically (17,18). Another study reported that the sensory conduction of the median nerve was diminished during ischemia (19). Our data are consistent with this finding. Axonal conduction in the ischemic sympathetic nerve may be diminished as well as in sensory and motor nerves.

Dialysate NE response to KCl was suppressed during the period of ischemia, although NE content at muscle sympathetic nerve endings was preserved during ischemia. This result indicates that exocytotic NE-releasing function in muscle sympathetic nerve endings is suppressed during ischemia lasting for 75 min. Our previous study on myocardial ischemia reported that cardiac sympathetic nerve ending activity was instigated within 20 min of coronary occlusion, with marked NE efflux from axoplasma subsequently occurring (20). Thus, ischemia leads to different results for skeletal muscle and the myocardium. Further studies on the mechanisms underlying these differences are warranted.

Acute limb ischemia progressively decreased dialysate NE concentrations. Furthermore, in ischemic regions the carotid baroreflex-mediated NE-releasing function was impaired, and the KCl-induced exocytotic releasing function at muscle sympathetic nerve endings also deteriorated. These results might explain the reduction in the dialysate NE concentration during periods of ischemia.

Acknowledgements: This work was supported by Grants-in-Aid for Scientific Research (13470154, 13877114) from the Ministry of Education, Culture, Sports, Science and Technology; New Energy and Industrial Technology Development Organization; The Research Grants for Cardiovascular Disease (H13C-1) from the Ministry of Health, Labor and Welfare; the Promotion Fundamental Studies in Health Science of the Organization for Pharmaceutical Safety and Research of Japan.

REFERENCES

1. Lundberg G, Wahlberg E, Swedenborg J, Sundberg CJ, Ungerstedt U, Olofsson P. Continuous assessment of local metabolism by microdialysis in critical limb ischaemia. *Eur J Vasc Endovasc Surg* 2000;19:605–13.
2. Aldman A, Larsson J, Elfstrom J. Muscle energy stores in relation to clinical findings and outcome in acute arterial ischaemia of the lower leg. *Eur J Vasc Surg* 1987;1:415–20.
3. Schömig A, Dart AM, Dietz R, Mayer E, Kübler W. Release of endogenous catecholamines in the ischemic myocardium of the rat. *Circ Res* 1984;55:689–701.
4. Inoue H, Zipes DP. Time course of denervation of efferent sympathetic and vagal nerve after occlusion of the coronary artery in the canine heart. *Circ Res* 1988;62:1111–20.
5. Barker D, Saito M. Autonomic innervation of receptors and muscle fibres in cat skeletal muscle. *Proc R Soc Lond B Biol Sci* 1981;212: 317–32.
6. Hill JM, Adreani CM, Kaufman MP. Muscle reflex stimulates sympathetic postganglionic efferents innervating triceps surae muscles of cats. *Am J Physiol Heart Circ Physiol* 1996;271:H38–H43.
7. Kamiya A, Sugiyama Y, Iwase S, Mano T. Muscle sympathetic nerve activity and plasma norepinephrine during 6 degrees head-down bed rest. *Environ Med* 1998;42:159–62.
8. Esler M, Jennings G, Korner P, et al. Assessment of human sympathetic nervous system activity from measurement of norepinephrine turnover. *Hypertension* 1988;11:3–20.
9. Akiyama T, Yamazaki T, Ninomiya I. Differential regional responses of myocardial interstitial noradrenaline levels to coronary occlusion. *Cardiovasc Res* 1993;27:817–22.
10. Akiyama T, Yamazaki T, Ninomiya I. In vivo monitoring of myocardial interstitial norepinephrine by dialysis technique. *Am J Physiol Heart Circ Physiol* 1991;261:H1643–7.
11. Yamazaki T, Akiyama T, Shindo T. Routine high-performance liquid chromatographic determination of myocardial interstitial norepinephrine. *J Chromatogr B Biomed Sci Appl* 1995;670:328–31.
12. Tanaka E, Hattan N, Ando K, et al. Amelioration of microvascular myocardial ischemia by gene transfer of vascular endothelial growth factor in rabbits. *J Thorac Cardiovasc Surg* 2000;120: 720–8.
13. Takauchi Y, Yamazaki T, Akiyama T. Tyramine-induced endogenous noradrenaline efflux from in situ cardiac sympathetic nerve ending in cats. *Acta Physiol Scand* 2000;168:287–93.
14. O'Leary DS, Sheriff DD. Is the muscle metaboreflex important in control of blood flow to ischemic active skeletal muscle in dogs? *Am J Physiol Heart Circ Physiol* 1995;268:H980–6.
15. Tokunaga N, Yamazaki T, Akiyama T, Sano S, Mori H. In vivo monitoring of norepinephrine and its metabolites in skeletal muscle. *Neurochem Int* 2003;43:573–80.
16. Fern R, Harrison PJ. The relationship between ischaemic conduction failure and conduction velocity in cat myelinated axons. *Exp Physiol* 1994;79:571–81.
17. Nukada H, Dyck PJ. Acute ischemia causes axonal stasis, swelling, attenuation, and secondary demyelination. *Ann Neurol* 1987;22: 311–18.
18. Makitie J, Teravainen H. Peripheral nerve injury and recovery after temporary ischemia. *Acta Neuropathol (Berl)* 1977;37:55–63.
19. Nielsen VK, Kardel T. Temporospatial effects on orthodromic sensory potential propagation during ischemia. *Ann Neurol* 1981;9: 597–604.
20. Akiyama T, Yamazaki T. Myocardial interstitial norepinephrine and dihydroxyphenylglycol levels during ischemia and reperfusion. *Cardiovasc Res* 2001;49:78–85.

THE JOURNAL OF BIOLOGICAL CHEMISTRY
Vol. 278, No. 14, Issue of April 4, pp. 11828–11835, 2003
Printed in U.S.A.

Mutations of Arg^{440} and Gly^{455}/Gly^{456} Oppositely Change pH Sensing of Na^+/H^+ Exchanger 1*

Received for publication, December 30, 2002
Published, JBC Papers in Press, January 30, 2003, DOI 10.1074/jbc.M213243200

Shigeo Wakabayashi‡, Takashi Hisamitsu, Tianxiang Pang, and Munekazu Shigekawa

From the Department of Molecular Physiology, National Cardiovascular Center Research Institute, Suita, Osaka 565-8565 Japan

To identify important amino acid residues involved in intracellular pH (pH_i) sensing of Na^+/H^+ exchanger 1, we produced single-residue substitution mutants in the region of the exchanger encompassing the putative 11th transmembrane segment (TM11) and its adjacent intracellular (intracellular loop (IL) 5) and extracellular loops (extracellular loop 6). Substitution of Arg^{440} in IL5 with other residues except positively charged Lys caused a large shift in pH_i dependence of $^{22}Na^+$ uptake to an acidic side, whereas substitution of Gly^{455} or Gly^{456} within the highly conserved glycine-rich sequence of TM11 shifted pH_i dependence to an alkaline side. The observed alkaline shift was larger with substitution of Gly^{455} with residues with increasing sizes, suggesting the involvement of the steric effect. Interestingly, mutation of Arg^{440} (R440D) abolished the ATP depletion-induced acidic shift in pH_i dependence of $^{22}Na^+$ uptake as well as the cytoplasmic alkalinization induced by various extracellular stimuli, whereas with that of Gly^{455} (G455Q) these functions were preserved. These mutant exchangers did not alter apparent affinities for extracellular transport substrates Na^+ and H^+ and the inhibitor 5-(*N*-ethyl-*N*-isopropyl)amiloride. These results suggest that positive charge at Arg^{440} is required for normal pH_i sensing, whereas mutation-induced perturbation of the TM11 structure may be involved in the effects of Gly mutations. Thus, both Arg^{440} in IL5 and Gly residues in the conserved segment of TM11 appear to constitute important elements for proper functioning of the putative "pH_i sensor" of Na^+/H^+ exchanger 1.

The Na^+/H^+ exchangers (NHEs)[1] are plasma membrane transporters that regulate pH homeostasis, cell volume, and transepithelial Na^+ absorption (1–4). The activity of ubiquitous exchanger isoform NHE1 is controlled by various extrinsic factors including hormones, growth factors, pharmacological agents, and mechanical stimuli (1–4). These stimuli have been shown to enhance NHE1 activity by shifting its intracellular pH (pH_i) dependence to an alkaline side. This phenomenon is usually explained by assuming that there exists an allosteric regulatory site for intracellular protons in NHE1 that is distinct from the Na^+ or H^+ transport site and that external stimuli increase the affinity of such H^+ modifier site (Ref. 5; see Refs. 1–4 for reviews). Regulation of NHE1 by these stimuli has been reported to occur through a variety of signaling molecules, *i.e.* calcinuerin B homologous protein (6, 7), Ca^{2+}/calmodulin (8, 9), low molecular mass GTPases Ras and Rho (10–12), p42/44 mitogen-activated protein kinases (13), p90 ribosomal S6 kinase (14), 14-3-3 protein (15), Nck-interacting kinase (16), and phosphatidylinositol 4,5-bisphosphate (17). However, the interrelationship of these signaling molecules and the mechanism by which they modulate the interaction of the putative H^+ modifier site with intracellular protons is still unclear.

The NHE family members have similar overall structures, consisting of an N-terminal transmembrane domain (~500 amino acids) containing 12 membrane spanning segments and a C-terminal cytoplasmic regulatory domain (~300 amino acids) (1–3). We previously showed that deletion of the cytoplasmic domain of NHE1 greatly shifted the pH_i dependence of exchange to an acidic side, with the steep pH_i dependence of exchange being maintained (18). Furthermore, we have presented evidence that the cytoplasmic domain of NHE1 contains several subdomains, which increase or decrease the pH_i sensitivity (19). These data may be consistent with the idea that the putative H^+ modifier site exists within the N-terminal transmembrane domain and that the cytoplasmic domain regulates the accessibility of regulatory protons to the site. However, the structural basis for such an idea is largely unknown.

Based on the accessibility of introduced cysteine residues to sulfhydryl reagents, we have recently presented a new membrane topology model of NHE1 in which the exchanger consists of 12 transmembrane segments with N- and C-tails located in the cytosol (20), although a previous study reported the N-tail to be cleaved as a signal peptide during the exchanger biogenesis (21). In a subsequent cysteine-scanning mutagenesis study, we found that mutation of Tyr^{454} or Arg^{458} in a new transmembrane domain 11 (TM11) impaired the plasma membrane expression of NHE1 (22), suggesting the importance of these residues for proper folding of NHE1. Furthermore, our preliminary experiments suggested that some residues in TM11 regulate pH_i sensitivity. In addition, it was noted that TM11 contains a phylogenetically conserved Gly-rich segment (see Fig. 1*B*). These findings prompted us to study the functions of amino acid residues within TM11 and adjacent intracellular (IL5) and extracellular loops (EL6).

* This work was supported by Grant-in-Aid on Priority Areas 13142210 and Grant-in-Aid for Scientific Research 14580664 from the Ministry of Education, Science, and Culture of Japan, by a grant from the Organization of Pharmaceutical Safety and Research of Japan (Promotion of Fundamental Studies in Health Science), and by Health and Labour Sciences research grants, and Research on Advanced Medical Technology Grant nano-001. The costs of publication of this article were defrayed in part by the payment of page charges. This article must therefore be hereby marked "*advertisement*" in accordance with 18 U.S.C. Section 1734 solely to indicate this fact.

‡ To whom correspondence should be addressed: Dept. of Molecular Physiology, National Cardiovascular Center Research Institute, Fujishirodai 5-7-1, Suita, Osaka 565-8565, Japan. Tel.: 81-6-6833-5012; Fax: 81-6-6872-7485; E-mail: wak@ri.ncvc.go.jp.

[1] The abbreviations used are: NHE, Na^+/H^+ exchanger; pH_i, intracellular pH; TM, transmembrane domain; EIPA, 5-(*N*-ethyl-*N*-isopropyl)amiloride; IL, intracellular loop; EL, extracellular loop; CHP, calcineurin B homologous protein; MTSET, 2-trimethylammoniumethyl methanethiosulfonate.

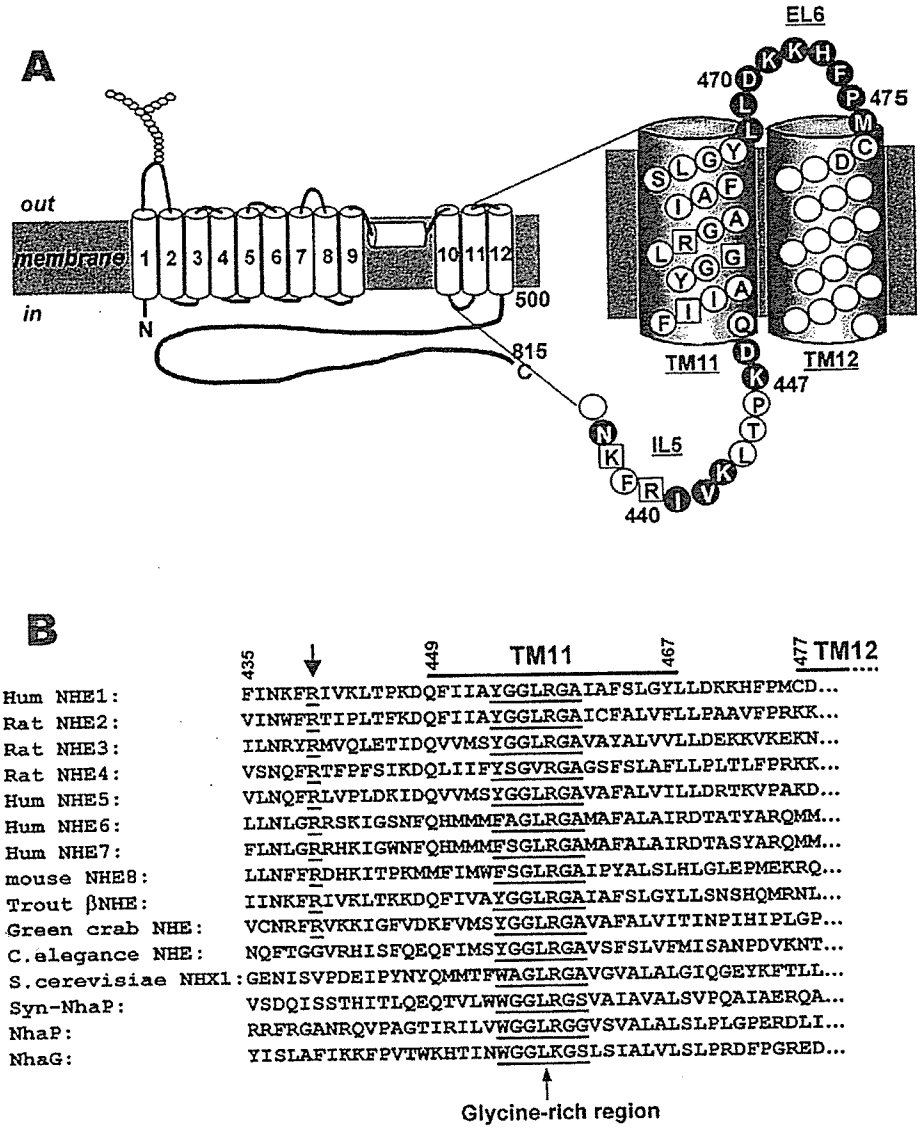

FIG. 1. **Topology of NHE1 and sequence alignment of TM11.** *A*, *left side*, a topological model of NHE1 based on our previous cysteine accessibility analysis (20). *Right side*, precise topologies of IL5, TMs 11 and 12, and EL6 revealed in this study. The positions examined for cysteine accessibility are represented by a single-letter amino acid code. *Black* and *gray circles* represent residues accessible to external and internal SH probes, respectively, whereas *white circles* represent residues not or only faintly labeled by biotin maleimide (see Fig. 2). *White squares* represent residues (Lys^{438}, Arg^{440}, Ile^{451}, Gly^{456}, and Arg^{458}) not studied here because cells expressing mutants could not be obtained. *B*, sequence alignment of TM11 and its neighboring regions in the exchangers from different species. GenBank™ accession numbers for these proteins are as follows: human NHE1, P19634; rat NHE2, NP_036785; rat NHE3, NP_036786; rat NHE4, P26434; human NHE5, NP_004585; human NHE6, NP_006350; human NHE7, NP_115980; mouse NHE8, NP_683731; trout βNHE, A46188; green crab NHE, AAC26968; *Caenorhabditis elegans* NHE, NP_509830; *Saccharomyces cerevisiae* NHX1, NP_010744; cynechobacterium (*Synechocystis sp.*) Syn-NhaP, NP_441245; *Pseudomonas aeruginosa* NhaP, NP_252576; and *Bacillus subtilis* NhaG, BAA89487.

In this study, we found that mutation of Arg^{440} within IL5 decreases the pH_i sensitivity, whereas mutation of Gly residues within the Gly-rich segment of TM11 increases it, suggesting that the region encompassing IL5 and TM11 is critical for the regulatory function of NHE1. This is the first identification of important residues involved in pH_i sensing within the transmembrane domain of NHE1.

EXPERIMENTAL PROCEDURES

Materials—Biotin maleimide was purchased from Molecular Probes Inc. MTSET and streptavidin-conjugated agarose were purchased from Toronto Research Chemicals Inc. and Pierce, respectively. Amiloride derivative 5-(*N*-ethyl-*N*-isopropyl)amiloride (EIPA) was a gift from the New Drug Research Laboratories of Kanebo, Ltd. (Osaka, Japan). $^{22}NaCl$ was purchased from PerkinElmer Life Sciences. An NHE1-specific polyclonal antibody (RP-cd) was raised as described previously (8). All other chemicals were of the highest purity available.

Cells, Culture Conditions, and Stable Expression—An Na^+/H^+ exchanger-deficient cell line (PS120) (23) and corresponding transfectants were maintained in Dulbecco' s modified Eagle' s medium (Invitrogen) containing 25 mM $NaHCO_3$ and supplemented with 7.5% (v/v) fetal calf serum, penicillin (50 units/ml), and streptomycin (50 μg/ml). The cells were maintained at 37 °C in the presence of 5% CO_2. PS120 cells (5×10^5 cells/100-mm dish) were transfected with each plasmid construct (20 μg) by the calcium phosphate co-precipitation technique. Cell populations that stably express mutant NHE1 were selected by the "H^+ killing" procedure as described (18).

Construction of Na^+/H^+ Exchanger Mutants—A plasmid carrying cDNA coding for the Na^+/H^+ exchanger (NHE1 human isoform) containing some unique restriction sites cloned into mammalian expression vector pECE was described previously (18). A cDNA construct for Cys-less NHE1 devoid of all endogenous cysteine residues was also described previously (20). For construction of point mutant cDNAs, we used a PCR-based strategy as described previously (20), using two template plasmids coding for the wild-type or Cys-less NHE1. Briefly,

using synthesized sense and antisense primers containing appropriate mutations, DNA fragments were generated by PCR. These fragments were digested and inserted into appropriate sites on the wild-type or Cys-less NHE1 plasmid. The DNA sequences of the PCR fragments were confirmed with a PerkinElmer Life Sciences model 373S autosequencer. We used the prefix "cl-" for point mutants produced from Cys-less NHE1 as a template.

Labeling with Biotin Maleimide—Biotin maleimide labeling of NHE1 mutant molecules was carried out as described previously (20). Briefly, confluent cells cultured on 60-mm dishes were washed twice with 5 ml of PBSCM (phosphate-buffered saline containing 0.1 mM $CaCl_2$ and 1 mM $MgCl_2$, pH 7.2) and then incubated in 1 ml of PBSCM containing 0 or 5 mM MTSET for 30 min at room temperature. The cells were washed twice with 5 ml of PBSCM and then incubated in 1 ml of PBSCM containing 0.5 mM biotin maleimide (100 mM stock in Me_2SO) for 30 min at room temperature. The cells were washed once with PBSCM containing 1% 2-mercaptoethanol, once with PBSCM, and then collected in the tube by centrifugation. The cells were solubilized with 1 ml of lysis buffer containing 1% Triton X-100, 150 mM NaCl, 20 mM Hepes/Tris (pH 7.4), 1 mM phosphate-buffered saline, and 1 mM benzamidine. After centrifugation for 10 min at 15,000 rpm, the supernatant was mixed with streptavidin-agarose beads (30 μl of resin), followed by incubation for 1 h at 4 °C with mild agitation. The agarose beads were washed more than five times with 1 ml of lysis buffer, mixed with 50 μl of SDS-PAGE sample buffer containing 3% SDS, and then boiled for 10 min at 100 °C. The proteins were separated on an 8.5% gel by SDS-PAGE and analyzed by immunoblotting with the NHE1 antibody as described previously (20). The blots were developed with an ECL detection system (Amersham Biosciences). When indicated, the cells were permeabilized with digitonin (50 μg/ml) or streptolysine O (Sigma) immediately before biotinylation, as described previously (20).

Measurement of $^{22}Na^+$ Uptake—$^{22}Na^+$ uptake activity and its pH_i dependence were measured by the K^+/nigericin pH_i clamp method (19). Serum-depleted cells in 24-well dishes were preincubated for 30 min at 37 °C in Na^+-free choline chloride/KCl medium containing 20 mM Hepes/Tris (pH 7.4), 1.2–140 mM KCl, 2 mM $CaCl_2$, 1 mM $MgCl_2$, 5 mM glucose, and 5 μM nigericin. In some experiments (see Fig. 6), the preincubation solution contained 2 μg/ml oligomycin and 5 mM 2-deoxyglucose instead of glucose. $^{22}Na^+$ uptake was started by adding the same choline chloride/KCl solution containing $^{22}NaCl$ (37 kBq/ml) (final concentration, 1 mM), 1 mM ouabain, and 100 μM bumetanide. In some wells, the uptake solution contained 0.1 mM EIPA. After 1 min, the cells were rapidly washed four times with ice-cold phosphate-buffered saline to terminate $^{22}Na^+$ uptake. pH_i was calculated from the imposed $[K^+]$ gradient by assuming the equilibrium $[K^+]_i/[K^+]_o = [H^+]_i/[H^+]_o$ and an intracellular $[K^+]$ of 120 mM. The data were normalized as to protein concentration, which was measured by bicinchoninic assay system (Pierce) using bovine serum albumin as a standard.

Measurement of Changes in pH_i—The changes in pH_i induced by various extracellular agents were measured by the [^{14}C]benzoic acid equilibration method, as described previously (18).

Statistics—The data for the pH dependence of $^{22}Na^+$ uptake were simulated by fitting the values to the sigmoidal dose-response equation, the rate of EIPA-sensitive $^{22}Na^+$ uptake $= V_{max}/(1 + 10^{(n(pK - pH_i))})$ (V_{max}, the maximal rate of $^{22}Na^+$ uptake; pK, pH_i giving half-maximal $^{22}Na^+$ uptake; n, Hill coefficient), with the aid of a simulation program included in the graphing software Graphpad Prizm (Microsoft Corp.). The concentration dependences of extracellular Na^+, pH, and EIPA for $^{22}Na^+$ uptake were also fitted to steady-state kinetic equations with the aid of the same simulation program. Kinetic parameters are expressed as the best fitted values with standard errors, whereas other data are expressed as the means ± S.D. for at least three determinations.

RESULTS

Precise Topology of the Putative 11th Transmembrane Domain and Neighboring Loops of NHE1—Based on the results of cysteine accessibility analysis, we previously presented a novel topology model of NHE1, as shown in Fig. 1*A* (20). Here, to obtain more precise topological information of the regions surrounding TM11, we introduced single Cys residues into these regions of Cys-less NHE1 and expressed mutants in the exchanger-deficient cells PS120. All of the mutant exchangers except cl-K438C, cl-R440C, cl-I451C, cl-G456C, and cl-R458C

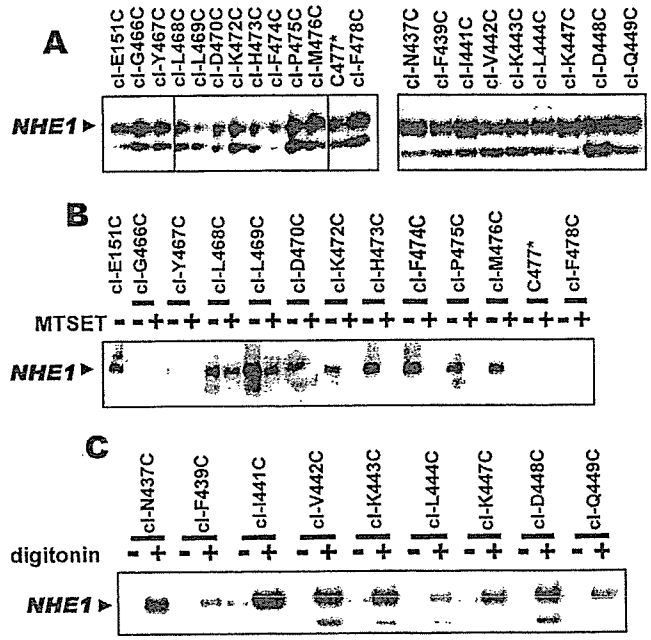

FIG. 2. **Biotinylation of neighboring regions of TM11.** Cells expressing single cysteine mutants of Cys-less NHE1 were treated with or without 5 mM MTSET. Then cells were incubated with 0.5 mM biotin maleimide, solubilized with lysis buffer, and treated with streptavidin-agarose as described under "Experimental Procedures." A total cell lysate (20 μg) (*A*) or the proteins recovered with streptavidin-agarose (*B* and *C*) were separated by SDS-PAGE, and the proteins were visualized by immunoblot analysis with an NHE1 antibody. In *C*, cells were permeabilized with digitonin before biotinylation also as described under "Experimental Procedures."

were well expressed in PS120 cells (Fig. 2*A*; also see Fig. 7 of Ref. 20). On SDS-PAGE, we observed two forms of exchanger protein with high (~110 kDa) and low (~90 kDa) molecular masses, which are thought to be a mature protein with *N*- and *O*-linked glycosylation and an immature protein containing only *N*-linked high mannose oligosaccharide, respectively (24). The cells were then incubated with 0.5 mM biotin maleimide after preincubation with or without a membrane-impermeable MTSET, and biotinylated proteins were subsequently recovered with streptavidin-agarose, followed by immunoblot analysis with an anti-NHE1 to visualize biotinylated exchangers (Fig. 2*B*).

Mutant exchangers cl-L468C, cl-L469C, cl-D470C, cl-K471C, cl-K472C, cl-H473C, cl-F474C, cl-P475C, and cl-M476C with high molecular mass were efficiently labeled with biotin maleimide (Fig. 2*B*; not shown for cl-K471C, but see Ref. 20). cl-E151C, used as a positive control, was also labeled, whereas Cys-less NHE1 was not (data not shown; see Ref. 20). The biotinylation of mutant exchangers was significantly inhibited by pretreatment with membrane-impermeable MTSET (Fig. 2*B*), suggesting that these residues face the outside. On the other hand, cl-G466C, cl-D478C, and Cys^{477}* (native cysteine) were not labeled with biotin maleimide, and cl-Y467C was only faintly labeled (Fig. 2*B*). In contrast, cl-N437C, cl-I441C, cl-V442C, cl-K443C, cl-K447C, and cl-D448C were labeled with biotin maleimide only when the cells were permeabilized with digitonin (Fig. 2*C*; data not shown for some mutants) or streptolysine O (see Ref. 20), suggesting that these positions face the inside. Some Cys mutants, *i.e.* cl-F439C, cl-L444C cl-T445C, cl-P446C, and cl-Q449C, were only faintly labeled even when cells were permeabilized with digitonin (Fig. 2*C*; data not shown for cl-T445C and cl-P446C). We found that introduced cysteines at Phe^{450}, Ile^{452}, Ala^{453}, Tyr^{454}, Gly^{455}, Leu^{457}, Gly^{459}, Ala^{460}, Ile^{461}, Ala^{462}, Phe^{463}, Ser^{464}, and Leu^{465} were

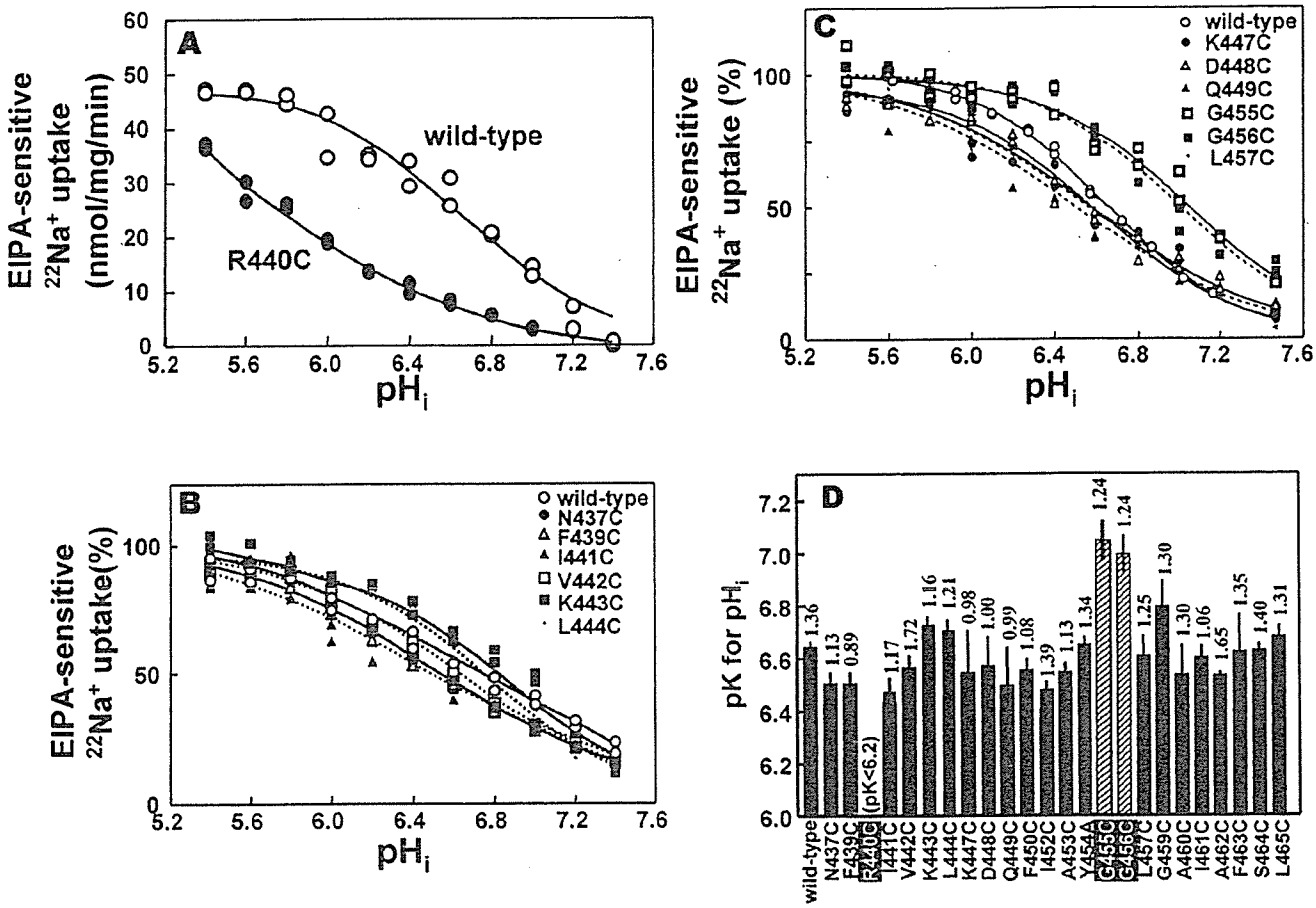

FIG. 3. **pH_i dependence of exchange activity in cells expressing various NHE1 cysteine mutants.** *A–C*, pH_i dependence of $^{22}Na^+$ uptake was measured in cells expressing the wild-type or cysteine mutant exchangers in the presence or absence of 0.1 mM EIPA. pH_i was clamped at various values with K^+/nigericin. The wild-type or mutant exchangers exhibited high $^{22}Na^+$ uptake activities (15–50 nmol/mg/min at pH_i 5.4). The data were fitted to the sigmoidal dose dependence equation as described under "Experimental Procedures." In *B* and *C*, the data were normalized to the maximal uptake activity. *D*, p*K* values obtained by curve fitting. The *bars* represent the standard errors given by the curve fitting program, whereas the *numbers* represent Hill coefficients.

not labeled with biotin maleimide in either intact or permeabilized cells (data not shown; see Ref. 20). Based on these results, we propose that: (i) the putative TM11 consists of 18 residues from Gln^{449} to Tyr^{467}, (ii) the putative TM12 starts from Cys^{477}, (iii) the region from Leu^{468} to Met^{476} forms the extracellular loop (EL6), (iv) the region from Asn^{437} to Asp^{448} forms part of the intracellular loop (IL5), and (v) some residues in IL5 may not be completely exposed to the cytosol. These topological data would be useful for the functional study of the exchanger in which residues in TM11 and its surrounding regions are mutated (see below).

Identification of Residues Modifying pH_i Sensitivity of NHE1—We introduced single Cys residues into the region covering most of IL5 and TM11 in the wild-type NHE1. In the wild-type background, R440C was well expressed in PS120 cells, but K438C, I451C, Y454C, and R458C were not. All Cys mutants expressed well in cells exhibited high EIPA-sensitive $^{22}Na^+$ uptake activity when cells were acidified. We found that substitution of Arg^{440} with Cys greatly shifted the pH_i dependence of $^{22}Na^+$ uptake to an acidic side with the p*K* of less than 6.2 (Fig. 3*A*). We could not determine the precise p*K* value for this mutant because of incomplete attainment of the maximal activity. On the other hand, mutations at other neighboring residues in IL5 did not significantly affect the pH_i dependence (Fig. 3*B*). Intriguingly, unlike the Arg^{440} mutation, mutations of Gly^{455} and Gly^{456} in TM11 significantly shifted the pH_i dependence of $^{22}Na^+$ uptake to an alkaline side, respectively (Fig. 3*C*). The p*K* values increased by ~0.3 pH units with these mutations. When these experiments were repeated more than three times, the p*K* values of mutant exchangers other than R440C, G455C, and G456C were in the range of 6.5–6.8, which is not very different from that of the wild-type NHE1 (Fig. 3*D*). Thus, we identified Arg^{440} in IL5 and Gly^{455}/Gly^{456} in TM11 as residues greatly influencing the pH_i sensitivity of NHE1.

We substituted Arg^{440} and Gly^{455} with other residues and analyzed the functional consequences of these mutations. Fig. 4 shows the pH_i dependence of $^{22}Na^+$ uptake in cells expressing R440D or R440K. Amino acid substitution of Arg^{440} with Asp greatly shifted the pH_i dependence to an acidic side. In the *inset* to Fig. 4, we present the ratios between the uptake activities of various substitution mutants of Arg^{440} at pH_i 6.8 and 5.4, in place of the respective pH_i dependences. The ratio decreased significantly when Arg^{440} was substituted with Lys, His, Asp, Glu, or Leu, indicating the acidic shift in the pH_i dependence. It is notable that the effect of the Arg^{440} to Lys substitution on the pH_i dependence was modest (p*K* = ~6.4) compared with the substitution with other residues (Fig. 4). Thus, the positive charge of Arg^{440} appears to be important for the normal pH_i sensitivity.

Fig. 5 (*A* and *B*) shows the results of amino acid substitution at Gly^{455}. Substitution of Gly^{455} to Gln, Thr, or Val significantly shifted the pH_i dependence of $^{22}Na^+$ uptake to an alkaline side, whereas substitution to Ala, Asp, Asn, or Ser did not shift or only modestly shifted. We plotted the p*K* values against

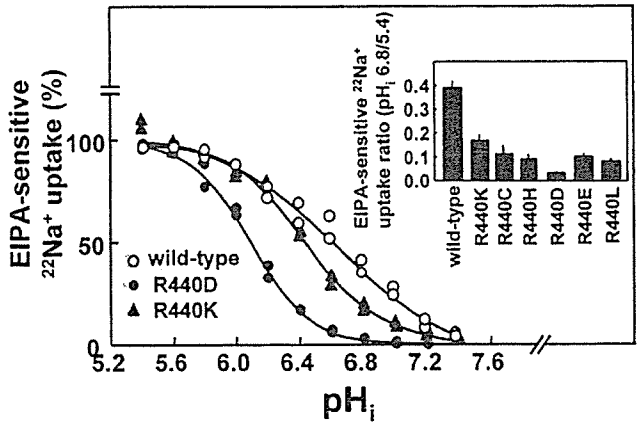

FIG. 4. **Effect of amino acid substitution at Arg^{440} on pH_i dependence of exchange activity.** pH_i dependences of EIPA-sensitive $^{22}Na^+$ uptake were compared among cells expressing the wild-type NHE1, R440K, and R440D. *Inset*, ratios between activities of various substitution mutants of Arg^{440} at pH_i 6.8 and 5.4 are presented. The cells expressing these exchangers exhibited high $^{22}Na^+$ uptake activities (20–45 nmol/mg/min at pH_i = 5.4). The data are the means ± S.D. of three determinations.

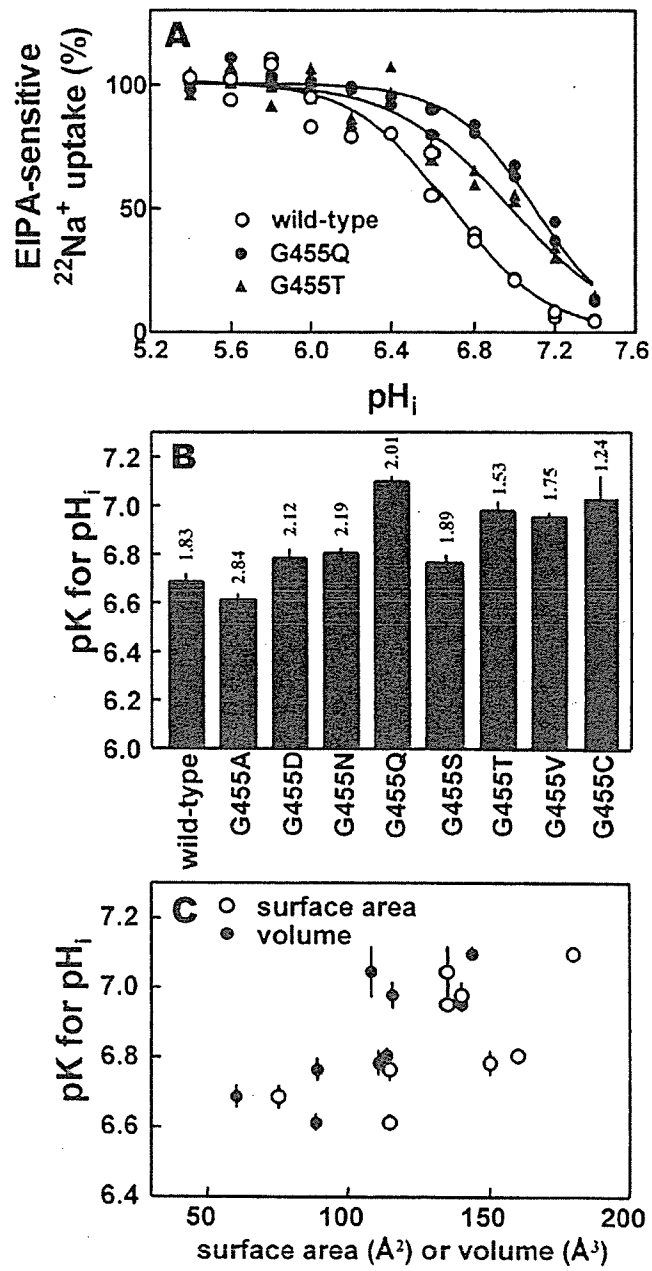

FIG. 5. **Effect of amino acid substitution at Gly^{455} on pH_i dependence of exchange activity.** *A*, pH_i dependence of $^{22}Na^+$ uptake was measured in cells expressing the wild-type or cysteine mutant exchangers in the presence or absence of 0.1 mM EIPA. The wild-type or mutant exchangers exhibited high $^{22}Na^+$ uptake activities (20–45 nmol/mg/min at pH_i = 5.4). *B*, p*K* values were obtained by curve fitting as described under "Experimental Procedures." The *bars* represent the standard errors given by the curve fitting program, whereas the numbers represent Hill coefficients. *C*, p*K* values were plotted against the surface area (43) or volume (44) of substituted amino acid side chains.

the surface area or volume of substituted amino acid side chains. The data suggest that the pK increases when Gly^{455} is substituted with bulky residues (Fig. 5*C*).

Mutations of Arg^{440} and Gly^{455} Do Not Change the Apparent Affinities for Extracellular Na^+, H^+, and EIPA—We analyzed several other kinetic parameters of Na^+/H^+ exchange in cells expressing R440D and G455Q that exhibited acidic and alkaline pH_i dependence of $^{22}Na^+$ uptake, respectively. Fig. 6 (*A–C*) shows the extracellular Na^+ concentration dependence of EIPA-sensitive $^{22}Na^+$ uptake. The K_m values for Na^+ estimated from double reciprocal plots (Fig. 6, *A–C*, *insets*) were similar for the wild-type NHE1 (9.22 ± 1.04 mM), R440D (9.30 ± 0.90 mM), and G455Q (14.08 ± 1.75 mM). The dependences of $^{22}Na^+$ uptake on extracellular pH (pH_o) and on the EIPA concentration were also similar for the wild-type NHE1, R440D, and G455Q (p*K* for pH_o, 7.29 ± 0.03, 7.50 ± 0.08, and 7.38 ± 0.02; IC_{50} for EIPA, 106.3 ± 7.3, 91.2 ± 0.1, and 85.0 ± 8.0 nM, respectively). The data suggest that mutations of Arg^{440} and Gly^{455} only affect the pH_i dependence of exchange.

Effects of Mutations of Arg^{440} and Gly^{455} on Some NHE Regulatory Functions—Cellular ATP depletion is known to inhibit the exchange activity by reducing the pH_i sensitivity and/or maximal activity (18, 25–28). Fig. 7 (*A* and *B*) shows the effect of ATP depletion on the pH_i dependence of $^{22}Na^+$ uptake in cells expressing R440D or G455Q. Interestingly, ATP depletion did not change the pH_i sensitivity in cells expressing R440D (Fig. 7*A*), although it caused ~50% reduction of V_{max} (data not shown). In contrast, ATP depletion greatly shifted the pH_i dependence of cells expressing G455Q to an acidic side without a change in V_{max}. However, it is notable that even under ATP depletion G455Q exhibited more alkaline pH_i dependence of $^{22}Na^+$ uptake (p*K*, ~6.4) compared with the wild type (p*K*, ~6.0).

Finally, we measured the changes in pH_i caused by various extracellular stimuli. In cells expressing the wild-type NHE1 and G455Q, we detected cytoplasmic alkalinization induced by thrombin, platelet-derived growth factor BB, hyperosmotic stress (sucrose), phorbol 12-myristate 13-acetate, lysophosphatidic acid, and the recently described activator Li^+ (29), indicating that all of these stimuli are capable of activating exchangers (Fig. 8). Of note, the extent of cytoplasmic alkalinization caused by hyperosmotic stress or Li^+ was reduced in cells expressing G455Q. In contrast, such alkalinization by extracellular stimuli was not observed in cells expressing R440D. Lack of alkalinization was presumably due to the acidic shift of the pH_i dependence of activity of R440D.

DISCUSSION

In this study, after obtaining precise information on the topology of the portion of NHE1 encompassing TM11 and its surrounding regions, we performed scanning mutagenesis analysis of these regions to search for residues possibly in-

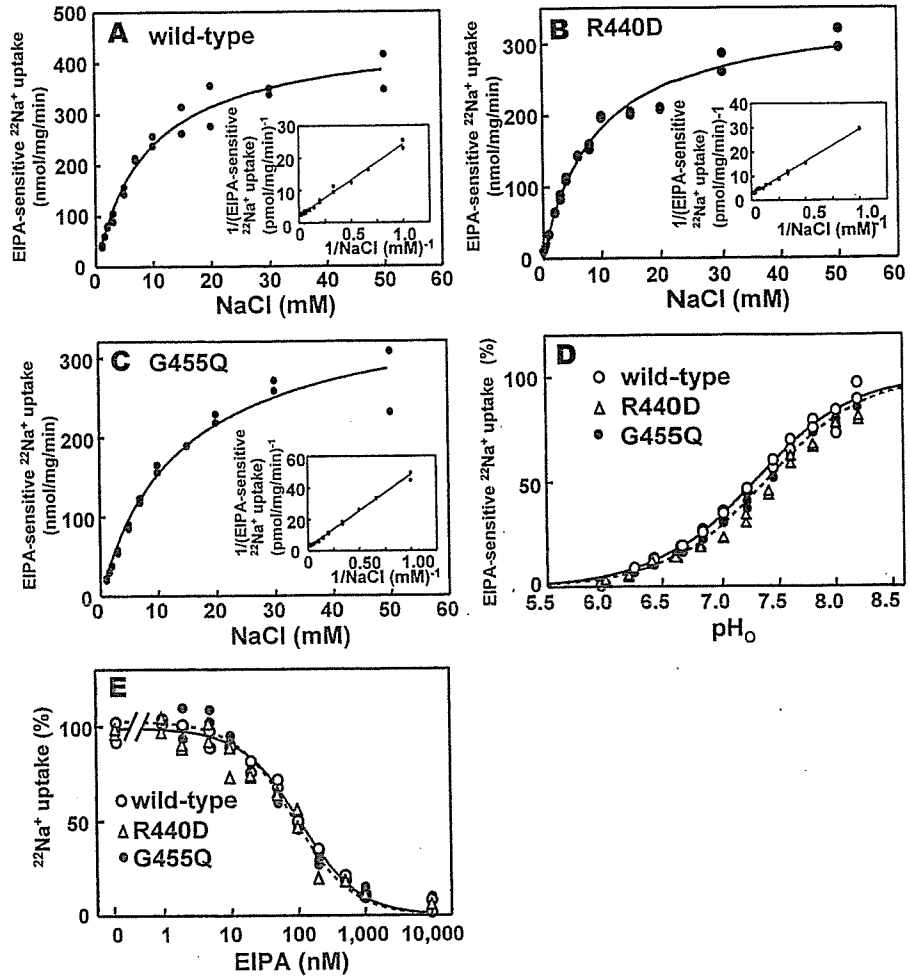

FIG. 6. **Comparison of kinetic properties of wild-type and mutant exchangers.** *A–C*, EIPA-sensitive $^{22}Na^+$ uptake in cells expressing the wild-type NHE1, R440D, or G455Q was measured as a function of Na^+ concentration. *Insets*, double reciprocal plots of exchange activity *versus* Na^+ concentration. *D* and *E*, EIPA-sensitive $^{22}Na^+$ uptake in cells expressing the wild-type NHE1, R440D, or G455Q was measured as a function of extracellular pH or EIPA concentration.

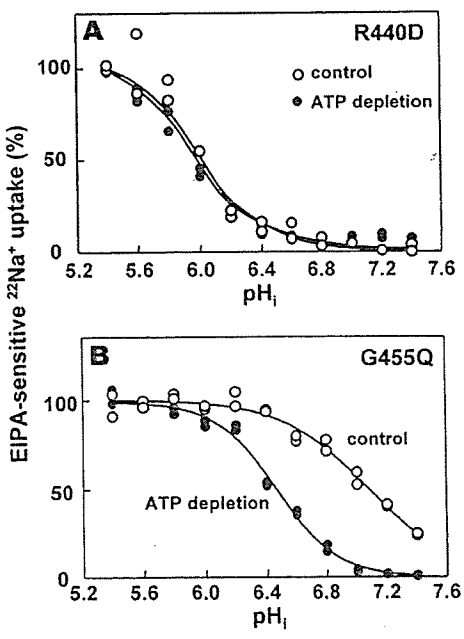

FIG. 7. **Effect of ATP depletion on pH_i dependence of exchange activity in cells expressing R440D or G455Q.** *A* and *B*, pH_i dependence of EIPA-sensitive $^{22}Na^+$ uptake was measured under control (*open circles*) or ATP-depleted conditions (*closed circles*) in cells expressing R440D or G455Q, respectively. In each panel, exchange activities are normalized to the ones measured at pH_i of 5.4.

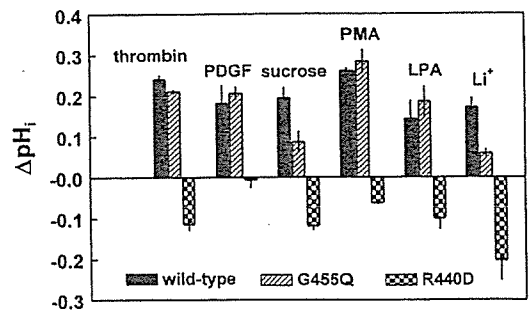

FIG. 8. **Extracellular stimuli-induced changes in pH_i in cells expressing the wild-type and mutant exchangers.** Changes in pH_i were measured as described under "Experimental Procedures" using the [^{14}C]benzoic acid equilibration method. The cells expressing the wild type, G455Q, or R440D were stimulated for 15 min at 37 °C with 2 units/ml thrombin, 10 ng/ml platelet-derived growth factor (*PDGF*) BB, 200 mM sucrose, 1 μM phorbol 12-myristate 13-acetate (*PMA*), 10 μg/ml lysophosphatidic acid, or 140 mM Li^+. For stimulation with Li^+, the cells were transferred from Hepes-buffered Dulbecco' s modified Eagle' s medium to medium containing 140 mM LiCl, 5 mM KCl, 2 mM $CaCl_2$, 1 mM $MgCl_2$. and 20 mM Hepes/Tris (pH 7.0).

volved in the regulation of pH_i dependence of Na^+/H^+ exchange. We found that mutation at Arg^{440} of IL5 of NHE1 greatly shifted pH_i dependence of EIPA-sensitive $^{22}Na^+$ uptake to an acidic side, whereas mutation at Gly^{455} or Gly^{456} of TM11 shifted it to an alkaline side. Mutation of many other residues in IL5 and TM11, in which it did not impair exchanger expression in the plasma membrane, did not alter the pH_i depend-

ence. Furthermore, these arginine and glycine mutations did not alter the apparent affinities of NHE1 for external transport substrates Na^+ and H^+ and the inhibitor EIPA. We observed similar opposite shifts of the pH_i dependence with these NHE1 mutants when we measured the reverse mode of Na^+/H^+ exchange, *i.e.* EIPA-sensitive $^{22}Na^+$ efflux from ^{22}Na-loaded cells,[2] supporting the possibility that the mutations alter the interaction of intracellular protons with the H^+ modifier site rather than the transport site. It thus appears likely that these single mutations exert rather specific effects on the pH_i sensor of NHE1.

In addition to the effect on pH_i dependence of basal Na^+/H^+ exchange, mutation of Arg^{440} abolished the ATP depletion-induced acidic shift of pH_i dependence of exchange activity as well as the cytoplasmic alkalinization in response to various extracellular stimuli. We previously reported (18) that deletion of the entire C-terminal cytoplasmic domain of NHE1 causes a large acidic shift of pH_i dependence of basal exchange activity and the disappearance of growth factor-induced cytoplasmic alkalinization. The same deletion was also found to abolish the ATP depletion-induced acidic shift of pH_i dependence of exchange activity. We subsequently provided evidence that these effects occur because of deletion of the N-terminal portion of the cytoplasmic domain of NHE1 named subdomain I (amino acids 503–600) (19). Thus, the effects caused by deletion of subdomain I and single mutation of Arg^{440}, which is localized in the internal loop (IL5) connecting TMs 10 and 11, are very similar except that in the latter the V_{max} of exchange activity is somewhat reduced by ATP depletion.

Recently, we have reported that the calcineurin B homologous protein CHP is an essential co-factor for the expression of high physiological levels of exchange activity in many plasma membrane NHE isoforms (6). We showed that CHP is tightly bound to a short juxtamembrane segment of the exchanger (amino acids 510–530 of subdomain I in the case of NHE1) (6). Interestingly, in addition to the large reduction of V_{max}, CHP binding-defective NHE1 mutants exhibited a marked shift of the pH_i dependence to an acidic side.[3] Thus, the mutation at Arg^{440}, deletion of subdomain I, and the CHP binding-defective mutation all caused the same effect, *i.e.* a marked shift of the pH_i dependence to the acidic side, suggesting that the region of IL5 containing Arg^{440} and the CHP-subdomain I complex are both involved in the preservation of physiological pH_i sensitivity of the exchanger. In this study, we observed that pH_i dependence of exchange activity did not change extensively by substitution of Arg^{440} with similarly charged but somewhat more bulky Lys residue, unlike substitutions with other residues (Cys, His, Asp, Glu, and Leu). This suggests that the positive charge of Arg^{440} is important. An attractive hypothesis would be that Arg^{440} interacts with negatively charged residue(s) localized in the CHP-subdomain I complex and that its substitution with other residues or cell ATP depletion results in the disruption of such interaction, thereby altering pH_i sensitivity of the exchanger. Consistent with this hypothesis, there is a cluster of acidic amino acid residues on the side opposite to one where CHP binds to NHE1 in a predicted model of CHP structure.[2]

As opposed to the mutation of Arg^{440} in IL5, mutation of Gly^{455} or Gly^{456} in the glycine-rich region within TM11 shifted the pH_i dependence of basal exchange activity to an alkaline side. Furthermore, in the Gly^{455} mutant, ATP depletion was able to induce a large acidic shift of the pH_i dependence without a change in V_{max}, a pattern mimicking that of the wild-type NHE1, although the pH_i dependence itself was shifted to the alkaline side under these conditions (Fig. 7*B*). In the same mutant, we observed normal cytoplasmic alkalinization in response to growth factors (Fig. 8). Thus, the underlying mechanisms for the effects of these Gly mutations and that of the Arg^{440} mutation in IL5 are likely to be different.

The glycine-rich region in TM11 of NHE1 is remarkably conserved in different types of NHEs from bacteria to mammals (Fig. 1*B*), suggesting its importance for the NHE function. Glycine has been suggested to serve as a molecular hinge permitting the occurrence of conformational changes of intramembrane helices in some proteins (30, 31) or as a notch for orienting multiple helices at the point of closest packing between membrane helices in several polytopic membrane proteins (32). In this study, we observed a clear tendency showing that substitution of Gly^{455} with more bulky residues are more effective in causing an alkaline shift of pH_i dependence of exchange activity (Fig. 5*C*), which indicates that small residues are required at the position of Gly^{455} for normal pH_i sensitivity. This appears to be in line with the fact that some isoforms such as NHEs 4, 6, 7, and 8 have small residues such as alanine and serine at this position (Fig. 1*B*). We previously found that single cysteine substitutions at Tyr^{454} and Arg^{458}, both being close to Gly^{455} or Gly^{456} in TM11, cause the retention of NHE1 protein in the endoplasmic reticulum (22), suggesting that these mutations impair proper protein folding. On the other hand, mutation of Gly^{455} neither prevented the plasma membrane expression of NHE1 protein nor appeared to alter other transport functions of the exchanger significantly. Based on all these pieces of information, we speculate that a relatively mild change in helix packing interaction of TM 11 with other transmembrane helice(s) was induced by the mutation at Gly^{455} or Gly^{456}, which indirectly modified the conformation and function of the putative H^+-regulatory site(s). It is noteworthy that in *Escherichia coli* antiporter NhaA distantly related to mammalian NHEs, mutation of Gly^{338} in the glycine-rich region of TM11 was reported to render the antiporter active in the wide range of pH, *i.e.* practically independent of the pH level between pH 6 and 9 (33).

Although the present and previous results suggest important roles of IL5, TM11, and the subdomain I-CHP complex in the modulation of pH_i sensing in NHE1, little is known about structures of the ion transport sites and the putative pH sensor and their interaction. In our previous study of membrane topology of NHE1, we found re-entrant loop-like structures between TMs 4 and 5, between TMs 8 and 9, and between TMs 9 and 10 (20). In addition, both TM4 and TM9 have been shown to be important for the interaction of NHE1 with amiloride analogue inhibitors that compete with the transport substrate Na^+ (34–38). Furthermore, other studies identified a few polar amino acid residues required for ion exchange within transmembrane segments in the mammalian NHE1 (38, 39) as well as in the Na^+/H^+ antiporters from *E. coli* (40, 41) and *Vibrio alginolyticus* (42). Much further study is required for the elucidation of the structural aspect of Na^+/H^+ exchange.

In summary, we have presented evidence that Arg^{440} in IL5 and Gly^{455} or Gly^{456} in TM11 are important residues that oppositely regulate the pH_i sensitivity of NHE1. This is the first identification of critical residues involved in pH_i sensing within the N-terminal transmembrane domain of NHE1.

[2] S. Wakabayashi, unpublished observations.
[3] T. Pang, unpublished observation.

REFERENCES

1. Wakabayashi, S., Shigekawa M., and Pouysségur, J. (1997) *Physiol. Rev.* **77**, 51–74
2. Orlowski J., and Grinstein, S. (1997) *J. Biol. Chem.* **272**, 22373–22376
3. Counillon, L., and Pouysségur, J. (2000) *J. Biol. Chem.* **275**, 1–4
4. Grinstein, S., Rotin, D., and Mason, M. J. (1989) *Biochim. Biophys. Acta* **988**, 73–97
5. Aronson, P, S., Nee, J., and Suhm, M. A. (1982) *Nature* **299**, 161–163

6. Lin, X., and Barber, D. L. (1996) *Proc. Natl. Acad. Sci. U. S. A.* **93,** 12631–12636
7. Pang, T., Su, X., Wakabayashi, S., and Shigekawa, M. (2001) *J. Biol. Chem.* **276,** 17367–17372
8. Bertrand, B., Wakabayashi, S., Ikeda, T., Pouysségur, J., and Shigekawa, M. (1994) *J. Biol. Chem.* **269,** 13703–13709
9. Wakabayashi, S., Bertrand, B., Ikeda, T., Pouysségur, J., and Shigekawa, M. (1994) *J. Biol. Chem.* **269,** 13710–13715
10. Voyno-Yasenetskaya, T., Conklin, B. R., Gilbert, R. L., Hooley, R., Bourne, H. R., and Barber, D. L. (1994) *J. Biol. Chem.* **269,** 4721–4724
11. Dhanasekaran, N., Prasad, M. V., Wadsworth, S. J., Dermott, J. M., and Van Rossum, G. (1994) *J. Biol. Chem.* **269,** 11802–11806
12. Hooley, R., Yu, C.-Y., Symons, M., and Barber, D. L. (1996) *J. Biol. Chem.* **271,** 6152–6158
13. Bianchini, L., L'Allemain, G., and Pouysségur, J. (1997) *J. Biol. Chem.* **272,** 271–279
14. Takahashi, E., Abe, J.-I., Gallis, B., Aebersold, R., Spring, D. J., Krebs, E. G., and Berk, B. C. (1999) *J. Biol. Chem.* **274,** 20206–20214
15. Lehoux, S., Abe, J. I., Florian, J. A., and Berk, B. C. (2001) *J. Biol. Chem.* **276,** 15794–15800
16. Yan, W., Nehrke, K., Choi, J., and Barber, D. L. (2001) *J. Biol. Chem.* **276,** 31349–31356
17. Aharonovitz, O., Zaun, H. C., Balla, T., York, J. D., Orlowski, J., and Grinstein, S. (2000) *J. Cell Biol.* **150,** 213–224
18. Wakabayashi, S., Fafournoux, P., Sardet, C., and Pouysségur, J. (1992) *Proc. Natl. Acad. Sci. U. S. A.* **89,** 2424–2428
19. Ikeda, T., Schmitt, B., Pouysségur, J., Wakabayashi, S., and Shigekawa, M. (1997) *J. Biochem. (Tokyo)* **121,** 295–303
20. Wakabayashi, S., Pang, T., Su, X., and Shigekawa, M. (2000) *J. Biol. Chem.* **275,** 7942–7949
21. Miyazaki, E., Sakaguchi, M., Wakabayashi, S., Shigekawa, M., and Mihara, K. (2001) *J. Biol. Chem.* **276,** 49221–49227
22. Wakabayashi, S., Pang, T., Su, X., and Shigekawa, M. (2000) *FEBS Lett.* **487,** 257–261
23. Pouysségur, J., Sardet, C., Franchi, A., L'Allemain, G., and Paris, S. (1984) *Proc. Natl. Acad. Sci. U. S. A.* **81,** 4833–4837
24. Counillon, L., Pouysségur, J., and Reithmeier, R. A. F. (1994) *Biochemistry* **33,** 10463–10469
25. Cassel, D., Katz, M., and Rotman, M. (1986) *J. Biol. Chem.* **261,** 5460–5466
26. Orlowski, J. (1993) *J. Biol. Chem.* **268,** 16369–16377
27. Yun, C. H. C., Tsé, C. M., and Donowitz, M. (1995) *Proc. Natl. Acad. Sci. U. S. A.* **92,** 10723–10727
28. Goss, G. G., Woodside, M., Wakabayashi, S., Pouysségur, J., Waddell, T., Downey, G. P., and Grinstein, S. (1994) *J. Biol. Chem.* **269,** 8741–8748
29. Kobayashi, Y., Pang, T., Iwamoto, T., Wakabayashi, S., and Shigekawa, M. (2000) *Pfluegers Arch. Eur. J. Physiol.* **439,** 455–462
30. Youxing, J., Lee, A., Chen, J., Cadene, M., Chait, B. T., and MacKinnon, R. (2002) *Nature* **417,** 523–526
31. Toyoshima, C., and Nomura, H. (2002) *Nature* **418,** 605–611
32. Javadpour, M. M., Eilers, M., Groesbeek, M., and Smith, S. O. (1999) *Biophys. J.* **77,** 1609–1618
33. Rimon, A., Gerchman, Y., Kariv, Z., and Padan, E. (1998) *J. Biol. Chem.* **273,** 26470–26476
34. Wang, D., Balkovetz, D. F., and Warnock, D. G. (1995) *Am. J. Physiol.* **269,** C392–C402
35. Counillon, L., Franchi, A., and Pouysségur, J. (1993) *Proc. Natl. Acad. Sci. U. S. A.* **90,** 4508–4512
36. Counillon, L., Noël, J., Reithmeier, R. A. F., and Pouysségur, J. (1997) *Biochemistry* **36,** 2951–2959
37. Orlowski, J., and Kandasamy, R. A. (1996) *J. Biol. Chem.* **271,** 19922–19927
38. Khadilkar, A., Iannuzzi, P., and Orlowski, J. (2001) *J. Biol. Chem.* **276,** 43792–43800
39. Fafournoux, P., Noel, J., and Pouysségur, J. (1994) *J. Biol. Chem.* **269,** 2589–2596
40. Noumi, T., Inoue, H., Sakurai, T., Tsuchiya, T., and Kanazawa, H. (1997) *J. Biochem. (Tokyo)* **121,** 661–670
41. Inoue, H., Noumi, T., Tsuchiya, T., and Kanazawa, H. (1995) *FEBS Lett.* **363,** 264–268
42. Nakamura, T., Komano, Y., and Unemoto, T. (1995) *Biochim. Biophys. Acta* **1230,** 170–176
43. Chothia, C. (1976) *J. Mol. Biol.* **105,** 1–14
44. Zamyatnin, A. A. (1972) *Prog. Biophys. Mol. Biol.* **24,** 107–123

THE JOURNAL OF BIOLOGICAL CHEMISTRY
Vol. 278, No. 44, Issue of October 31, pp. 43580–43585, 2003
Printed in U.S.A.

Kinetic Dissection of Two Distinct Proton Binding Sites in Na^+/H^+ Exchangers by Measurement of Reverse Mode Reaction*

Received for publication, June 24, 2003, and in revised form, July 24, 2003
Published, JBC Papers in Press, August 19, 2003, DOI 10.1074/jbc.M306690200

Shigeo Wakabayashi‡, Takashi Hisamitsu, Tianxiang Pang, and Munekazu Shigekawa

From the Department of Molecular Physiology, National Cardiovascular Center Research Institute, Suita, Osaka 565-8565 Japan

We examined the effect of intracellular acidification on the reverse mode of Na^+/H^+ exchange by measuring $^{22}Na^+$ efflux from $^{22}Na^+$-loaded PS120 cells expressing the Na^+/H^+ exchanger (NHE) isoforms NHE1, NHE2, and NHE3. The 5-(*N*-ethyl-*N*-isopropyl)amiloride (EIPA)- or amiloride-sensitive fraction of $^{22}Na^+$ efflux was dramatically accelerated by cytosolic acidification as opposed to thermodynamic prediction, supporting the concept that these NHE isoforms are activated by protonation of an internal binding site(s) distinct from the H^+ transport site. Intracellular pH (pH_i) dependence of $^{22}Na^+$ efflux roughly exhibited a bell-shaped profile; mild acidification from pH_i 7.5 to 7 dramatically accelerated $^{22}Na^+$ efflux, whereas acidification from pH_i 6.6 gradually decreased it. Alkalinization above pH_i 7.5 completely suppressed EIPA-sensitive $^{22}Na^+$ efflux. Cell ATP depletion and mutation of NHE1 at Arg^{440} (R440D) caused a large acidic shift of the pH_i profile for $^{22}Na^+$ efflux, whereas mutation at Gly^{455} (G455Q) caused a significant alkaline shift. Because these mutations and ATP depletion cause correspondingly similar effects on the forward mode of Na^+/H^+ exchange, it is most likely that they alter exchange activity by modulating affinity of the internal modifier site for protons. The data provide substantial evidence that a proton modifier site(s) distinct from the transport site controls activities of at least three NHE isoforms through cooperative interaction with multiple protons.

The Na^+/H^+ exchangers (NHEs)[1] belong to one of the secondary active transporter families that catalyze the transport of ions or solutes using a driving force generated by active ion pumps. NHEs are involved in various cellular functions such as pH homeostasis, cell volume regulation, and transepithelial Na^+ absorption (1–4), and at least eight isoforms differing in tissue and subcellular localization have been identified. The activities of NHEs are controlled by various extrinsic factors including hormones, growth factors, pharmacological agents, and mechanical stimuli (1–4). Many of these stimuli modulate the activity by changing the apparent affinity for intracellular H^+ (Refs. 5–8; see Refs. 1–4 for reviews).

Physiologically, NHE catalyzes an electroneutral exchange of extracellular Na^+ for intracellular H^+, *i.e.* a forward mode of exchange with the aid of a constant driving force provided by a Na^+ pump. However, NHE is also able to catalyze the exchange of intracellular Na^+ for extracellular H^+, *i.e.* a reverse mode of exchange under certain conditions. In cells, NHE is inactivated usually at an intracellular pH (pH_i) of ~7.2, a value much lower than that (>8) predicted from the thermodynamic equilibrium between intracellular and extracellular Na^+ and H^+ ions. This "set point" behavior has been attributed to the existence of an allosteric regulatory site(s) called the "H^+ modifier" site or "pH sensor" in NHE. Twenty years ago, Aronson *et al.* (9, 10) elegantly presented evidence for such a site based on analysis of the kinetics of ion exchange in renal brush border membrane vesicles; they found that $^{22}Na^+$ uptake into Na^+-loaded vesicles (Na^+/Na^+ exchange) is stimulated by intravesicular H^+ and that $^{22}Na^+$ efflux is stimulated by intravesicular H^+, a finding opposite to the expected competitive interaction of H^+ with Na^+. These findings led to the idea that NHE becomes active only when the internal H^+ modifier site is occupied by a proton. In many subsequent studies using native or NHE-transfected cells, exchange activity was reported to exhibit a complex, cooperative dependence on the internal H^+ concentration despite its hyperbolic dependence on external Na^+ or H^+ concentration (11–18), suggesting the involvement of at least two binding sites for internal H^+. However, because only the forward mode of exchange was measured in these studies and because very accurate measurement of pH_i is sometimes difficult, it still remains difficult to clearly distinguish the H^+ modifier and H^+ transport sites. Furthermore, it is not clear that the H^+ modifier site exists in various NHE isoforms, because detailed analysis has not yet been performed using cells expressing each NHE isoform.

To obtain insight into the modifier role of intracellular H^+, in this study we measured pH_i dependence of $^{22}Na^+$ efflux from cells expressing NHE1, NHE2, or NHE3. We found that $^{22}Na^+$ efflux is dramatically stimulated by intracellular acidification but almost completely inhibited by modest alkalinization (pH_i ~7.5), which provides a strong piece of evidence for the existence of an intracellular H^+ modifier site in these NHE isoforms. We show that pH_i dependence of the Na^+/H^+ exchange can be explained by assuming the interaction of multiple protons with the regulatory site(s) and the interaction of a single proton with the transport site.

EXPERIMENTAL PROCEDURES

Materials—The amiloride derivative 5-(*N*-ethyl-*N*-isopropyl)amiloride (EIPA) was a gift from New Drug Research Laboratories of Kanebo, Ltd. (Osaka, Japan). $^{22}NaCl$ was purchased from PerkinElmer Life Sciences. All other chemicals were of the highest purity available.

* This work was supported by Grant-in-Aid on Priority Areas 13142210 and Grant-in-Aid for Scientific Research 14580664 from the Ministry of Education, Science, and Culture of Japan, a grant from the Organization of Pharmaceutical Safety and Research (OPSR) of Japan (Promotion of Fundamental Studies in Health Science), Ministry of Health Labour Sciences research grants, and Research on Advanced Medical Technology Grant nano-001.The costs of publication of this article were defrayed in part by the payment of page charges. This article must therefore be hereby marked "*advertisement*" in accordance with 18 U.S.C. Section 1734 solely to indicate this fact.

‡ To whom correspondence should be addressed: Dept. of Molecular Physiology, National Cardiovascular Center Research Inst., Fujishirodai 5-7-1, Suita, Osaka 565-8565, Japan. Tel.: 81-6-6833-5012; Fax: 81-6-6872-7485; E-mail: wak@ri.ncvc.go.jp.

[1] The abbreviations used are: NHE, Na^+/H^+ exchanger; pH_i, intracellular pH; EIPA, 5-(*N*-ethyl-*N*-isopropyl)amiloride.

Cell Culture and Stable Expression—A Na^+/H^+ exchanger-deficient cell line (PS120) (19) and corresponding transfectants were maintained in Dulbecco' s modified Eagle' s medium (Invitrogen) as described (16). Plasmid transfection and selection of cell populations expressing NHE variants were performed as described (16).

Construction of Na^+/H^+ Exchanger Mutants—A plasmid carrying cDNA coding for the Na^+/H^+ exchanger isoforms NHE1–3 cloned into the mammalian expression vector pECE was described previously (16). The construction of two mutants, G455Q and R440D, was also described previously (20). Gly^{455} and Arg^{440} were reported to be located within the putative transmembrane-spanning domain 11 (TM11) and the intracellular loop 5 (IL5) connecting transmembrane domains 10 and 11 (20).

Measurement of $^{22}Na^+$ Efflux—Serum-depleted cells in 24-well dishes were loaded with $^{22}Na^+$ by preincubating them for 30 min at 37 °C in chloride/KCl medium comprising 20 mM Hepes/Tris (pH 7.4), 0.2–1.2 mM $^{22}NaCl$ (37 kBq/ml), 1.9–140 mM KCl, 2 mM $CaCl_2$, 1 mM $MgCl_2$, 5 mM glucose, and 5 μM nigericin. Choline chloride was added to the medium to maintain the total concentration of KCl plus choline chloride at 140 mM. After removal of the radioactive preincubation solution, $^{22}Na^+$ efflux was started by adding the same choline chloride/KCl medium except that it additionally contained 2 mM ouabain and 100 μM bumetanide but not $^{22}Na^+$. For the data at zero time, this efflux solution was not added. In some wells, the efflux solution contained 0.1 mM EIPA or 5 mM amiloride. At the times indicated in Figs. 1, 3, and 5, cells were rapidly washed four times with ice-cold PBS to terminate $^{22}Na^+$ efflux. pH_i was calculated from the imposed $[K^+]$ gradient by assuming the equilibrium $[K^+]_i/[K^+]_o = [H^+]_i/[H^+]_o$ and an intracellular $[K^+]$ of 120 mM. Data were normalized as to the protein concentration, which was measured with a bicinchoninic assay system (Pierce) using bovine serum albumin as a standard.

Measurement of $^{22}Na^+$ Uptake—$^{22}Na^+$ uptake activity was measured using serum-depleted cells grown in 24-well dishes in the presence or absence of EIPA as described previously (20).

RESULTS

To measure $^{22}Na^+$ efflux, we first preincubated PS120 cells or their NHE transfectants for 30 min in a radioactive solution containing 1 mM $^{22}NaCl$, the K^+/H^+ ionophore nigericin, and either 48 or 140 mM KCl. This preincubation allowed cells to be pH_i-clamped at 7 or 7.5 and, at the same time, to be loaded with $^{22}Na^+$. $^{22}Na^+$ was rapidly taken up by cells and reached nearly to the plateau after the preincubation for 20 min under both conditions (Fig. 1*B*), suggesting that the radioactivity of $^{22}Na^+$ was equilibrated in the extra- and intracellular medium. The intracellular $^{22}Na^+$ concentration at 30 min was 1–2 mM by assuming a value of 5 μl of cell water per milligram of protein. After removal of the preincubation solution, cells were placed in a Na^+-free, non-radioactive solution (pH 7.4) to start $^{22}Na^+$ efflux. By this procedure, we were able to measure $^{22}Na^+$ efflux in the presence of an outwardly directed H^+ gradient (at pH_i 7) or in almost the absence of the H^+ gradient (at pH_i 7.5) (Fig. 1*A*). We expected that NHE-independent background $^{22}Na^+$ leakage would be minimal, because the efflux medium contained the Na^+-pump inhibitor ouabain and the $Na^+/K^+/Cl^-$ cotransporter inhibitor bumetanide but not HCO_3^-, a substrate for both Na^+/HCO_3^- cotransporter and Na^+-dependent Cl^-/HCO_3^- exchanger. In fact, we observed only slow $^{22}Na^+$ efflux in exchanger-deficient PS120 cells and their NHE1 transfectants in the presence of the NHE-specific inhibitor EIPA (Fig. 1, *C–E*).

As expected, EIPA-sensitive $^{22}Na^+$ efflux was not detectable in exchanger-deficient PS120 cells whose pH_i was maintained at 7 (Fig. 1*C*) or 7.5 (not shown). In NHE1 transfectants, however, rapid EIPA-sensitive $^{22}Na^+$ efflux was observed at pH_i 7 (Fig. 1*D*), although little EIPA-sensitive $^{22}Na^+$ efflux was observed at pH_i 7.5 (Fig. 1*E*). Thus, $^{22}Na^+$ efflux via NHE1 is dramatically stimulated by intracellular acidification, whereas it is completely inhibited by alkalinization. If we assume that NHE1 catalyzes a counter transport reaction only involving the transport site, the outwardly directed H^+ gradient should lead to inhibition of $^{22}Na^+$ efflux. The data support the view that activity of NHE1 is regulated by protonation/deprotonation of

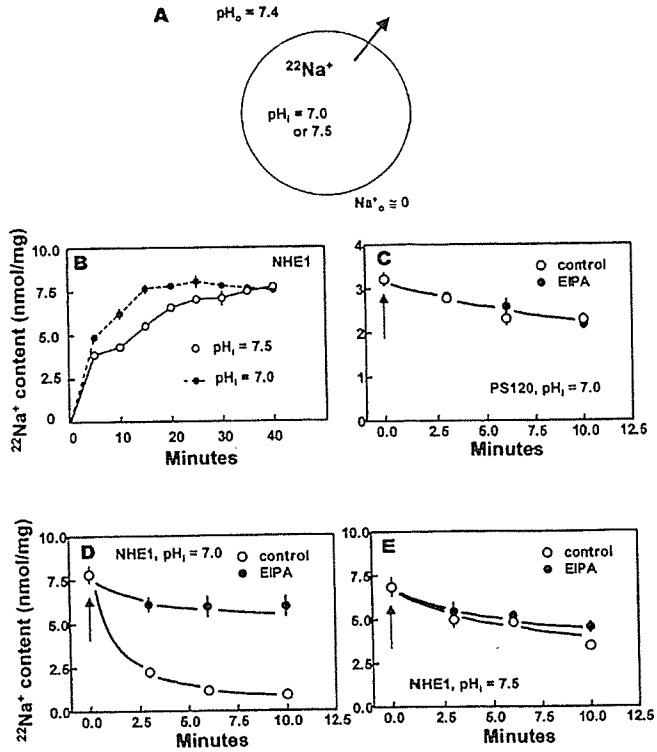

FIG. 1. **Time courses of $^{22}Na^+$ efflux from PS120 cells and their NHE1 transfectants.** PS120 cells or NHE1 transfectants were pH_i-clamped at 7 or 7.5 by incubating with 5 μM nigericin plus 48 or 140 mM KCl, respectively, as described under "Experimental Procedures." At the same time, $^{22}Na^+$ was loaded into the cells in the presence of 1 mM $^{22}NaCl$. After removal of the radioactive pH_i clamp solution, the cells were incubated in the Na^+-free non-radioactive efflux solution. *A*, illustration representing the intra- and extracellular ionic conditions in the $^{22}Na^+$ efflux experiment. pH_o, extracellular pH. *B*, time courses of $^{22}Na^+$ loading in PS120 cells expressing NHE1 measured at pH_i 7.5 (○) or 7 (●). *C*, time courses of $^{22}Na^+$ efflux in PS120 cells were measured in the presence (●) and absence (○) of 0.1 mM EIPA at pH_i 7. *D* and *E*, time courses of $^{22}Na^+$ efflux in cells expressing NHE1 were measured in the presence (●) and absence (○) of 0.1 mM EIPA at a pH_i of 7 and 7.5, respectively. Data represent means ± S.D. of three determinations.

the H^+ modifier site(s), which is different from the H^+ transport site.

To examine pH_i dependence of $^{22}Na^+$ efflux, we clamped pH_i at various values by incubating NHE1-expressing cells for 30 min in solutions containing nigericin and different concentrations of KCl. Because $^{22}Na^+$ was taken up by cells via the exchanger during pH_i clamping, $^{22}Na^+$ loading was greater in cells clamped at lower pH_i than in cells clamped at higher pH_i. To minimize such differences in $^{22}Na^+$ loading, we used a pH_i clamp solution containing different concentrations (0.2–1.2 mM) of $^{22}NaCl$. As shown in Fig. 2*A*, the level of $^{22}Na^+$ loading varied from 10 to 16 nmol/mg (corresponding to intracellular concentrations of 2–3 mM), indicating that the outwardly directed Na^+ gradient produced under the conditions used was not very different. Fig. 2*A* also shows levels of $^{22}Na^+$ remaining in cells 3 min after the addition of the efflux solution with or without EIPA. We plotted the EIPA-sensitive fraction of $^{22}Na^+$ efflux (Fig. 2*B*, *open circles*), and the values normalized to the initial level of $^{22}Na^+$ loading as a function of pH_i (Fig. 2*C*). The $^{22}Na^+$ efflux increased steeply with decreasing pH_i from 7.5 to 7.2, reached the maximum at pH_i 6.6, and then decreased with decreasing pH_i from 6.6 to 5.6. The bell-shaped pH_i profile of $^{22}Na^+$ efflux suggests that there are at least two intracellular proton-binding sites, each involved in the stimulation and inhibition of NHE1 function, respectively.

We examined the effect of cell ATP depletion on the pH_i

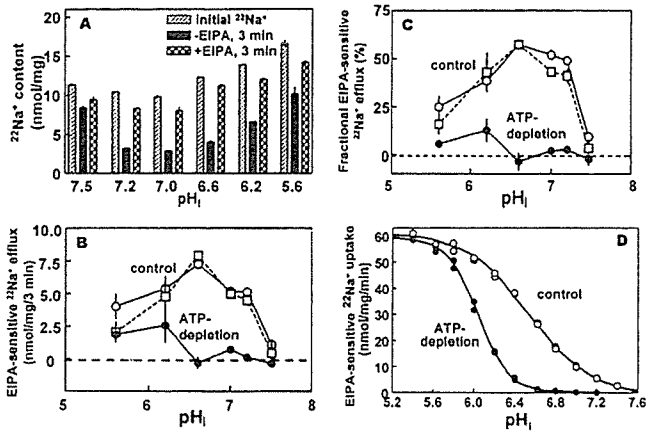

FIG. 2. **The pH_i profile of $^{22}Na^+$ efflux.** Cells expressing the wild-type NHE1 were pH_i-clamped with K^+/nigericin and, at the same time, loaded with $^{22}Na^+$ under control or ATP-depletion conditions as described under "Experimental Procedures." This preincubation solution contained 140, 76, 48, 19, 7.6, and 1.9 mM KCl and 0.2, 0.3, 0.5, 0.7, 0.9 and 1.2 mM $^{22}NaCl$ for pH_i values of 7.5, 7.2, 7, 6.6, 6.2 and 5.6, respectively. After removal of the radioactive preincubation solution, the cells were incubated in the Na^+-free non-radioactive efflux solution in the presence or absence of 0.1 mM EIPA. *A*, the intracellular contents of $^{22}Na^+$ present at the start of efflux and $^{22}Na^+$ remaining in cells at 3 min after the switch to the EIPA-free and EIPA-containing medium were plotted against pH_i. Data represent means ± S.D. of three determinations. *B*, absolute values of EIPA-sensitive $^{22}Na^+$ efflux (3 min) under control (○ and □) or ATP depletion conditions (●) were plotted against pH_i. For control, results from two independent experiments were represented, and one (○) was calculated from the data in *panel A*. *C*, EIPA-sensitive $^{22}Na^+$ efflux was normalized to the initial $^{22}Na^+$ content and then plotted against pH_i. Data represent means ± S.D. of three determinations. *D*, for comparison, pH_i dependence of $^{22}Na^+$ uptake is presented under control (○) or ATP-depletion conditions (●).

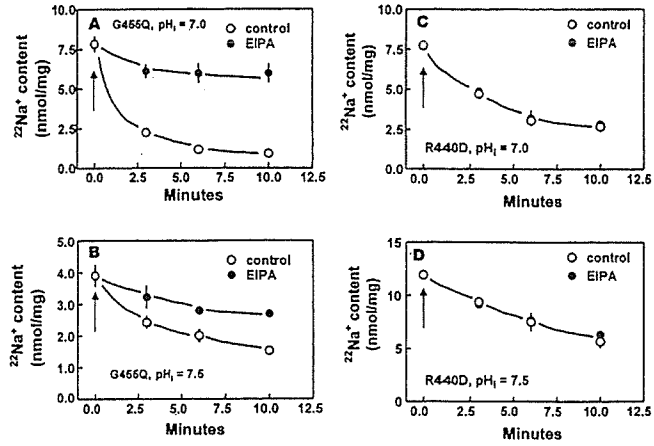

FIG. 3. **$^{22}Na^+$ efflux in cells expressing G455Q or R440D.** *A* and *B*, time courses of $^{22}Na^+$ efflux from cells expressing G455Q were measured in the presence (●) and absence (○) of 0.1 mM EIPA at pH_i 7 or 7.5, respectively, as described under "Experimental Procedures." *C* and *D*, time courses of $^{22}Na^+$ efflux from cells expressing R440D were measured in the presence (●) and absence (●) of 0.1 mM EIPA at pH_i 7 or 7.5, respectively. Data represent means ± S.D. of three determinations.

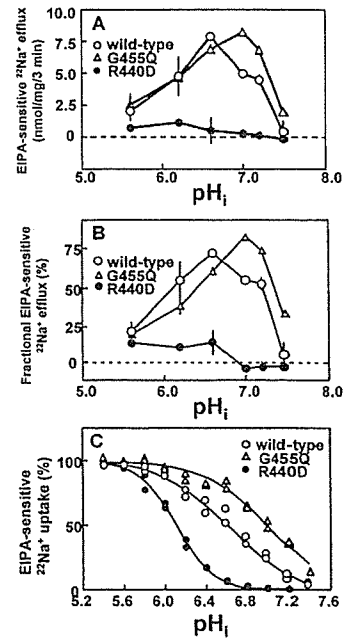

FIG. 4. **The pH_i profile of $^{22}Na^+$ efflux and $^{22}Na^+$ uptake in cells expressing G455Q or R440D.** *A*, cells expressing G455Q or R440D were pH_i-clamped with K^+/nigericin and, at the same time, loaded with $^{22}Na^+$ as described under "Experimental Procedures." The concentrations of KCl and $^{22}NaCl$ in preincubation solutions were the same as those given in the legend to Fig. 2. Absolute values of EIPA-sensitive $^{22}Na^+$ efflux (3 min) were plotted against pH_i. *B*, EIPA-sensitive $^{22}Na^+$ efflux was normalized to the initial $^{22}Na^+$ content and then plotted against pH_i. Data represent means ± S.D. of three determinations. *C*, for comparison, $^{22}Na^+$ uptake data were represented.

dependence of $^{22}Na^+$ efflux. We treated cells for 30 min with metabolic inhibitors 2-deoxyglucose (5 mM) and oligomycin (2 μg/ml) during pH_i clamping. Such treatment decreased cell ATP to less than 5% of that in normal cells (16). In these cells, the initial $^{22}Na^+$ loading was 6–9 nmol/mg (corresponding to intracellular concentrations of 1.2–1.8 mM) at pH_i values from 6.6 to 7.5, although $^{22}Na^+$ was loaded to high levels (20–30 nmol/mg) at pH_i 6.2 or 5.6. EIPA-sensitive $^{22}Na^+$ efflux and its normalized values were plotted against pH_i. As shown in Fig. 2, *B* and *C*, $^{22}Na^+$ efflux was almost completely inhibited by ATP depletion at least in the pH_i range from 6.6 to 7.5, consistent with the previous finding (16, 21–23) that ATP depletion greatly shifts the pH_i dependence of the forward mode of Na^+/H^+ exchange to an acidic side, as shown in Fig. 2*D*. It is also noted that, similar to the forward mode, the inhibitory effect of ATP-depletion on $^{22}Na^+$ efflux is alleviated by acidification.

Fig. 3 shows the results of similar $^{22}Na^+$ efflux measurements using cells expressing G455Q or R440D in which the pH_i dependence of the forward mode of exchange markedly shifts to alkaline and acidic sides, respectively (Fig. 4*B*; see also Ref. 20). As in the case with the wild type NHE1, $^{22}Na^+$ efflux in G455Q-expressing cells was much faster at pH_i 7 than at pH_i 7.5 (Fig. 3, *A* and *B*). Interestingly, a significant level of EIPA-sensitive $^{22}Na^+$ efflux was still observed in these cells even at pH_i 7.5 (Fig. 3*B*), unlike the case with the wild-type NHE1. In contrast, a significant level of EIPA-sensitive $^{22}Na^+$ efflux was not observed in R440D-expressing cells at pH_i 7 (Fig. 3*C*) or 7.5 (Fig. 3*D*), although low levels of $^{22}Na^+$ efflux were observed in a more acidic range of pH_i (Fig. 4*A*). Fig. 4 shows pH_i profiles of $^{22}Na^+$ efflux in cells expressing G455Q or R440D. The pH_i profile was significantly shifted to an alkaline side in G455Q-expressing cells compared with cells expressing the wild-type NHE1 (Fig. 4, *A* and *B*). In contrast, the pH_i profile was markedly shifted to an acidic side in cells expressing R440D.

Finally, we examined whether intracellular acidification activates $^{22}Na^+$ efflux in cells expressing NHE2 or NHE3 (Fig. 5). In these experiments, we used a high concentration (5 mM) of amiloride in place of EIPA as an inhibitor, because these isoforms are relatively less sensitive to the amiloride analogue. As in the case of NHE1, modest intracellular acidification (pH_i 7) significantly accelerated amiloride-sensitive $^{22}Na^+$ efflux from cells expressing NHE2 or NHE3, although $^{22}Na^+$ efflux from

NHE2 transfectants was relatively slow (Fig. 5). The slow efflux in NHE2 transfectants may be due to lower expression of the exchanger in the plasma membrane, because exchange activity of these transfectants was 20–30% of that of NHE1 or NHE3 transfectants.

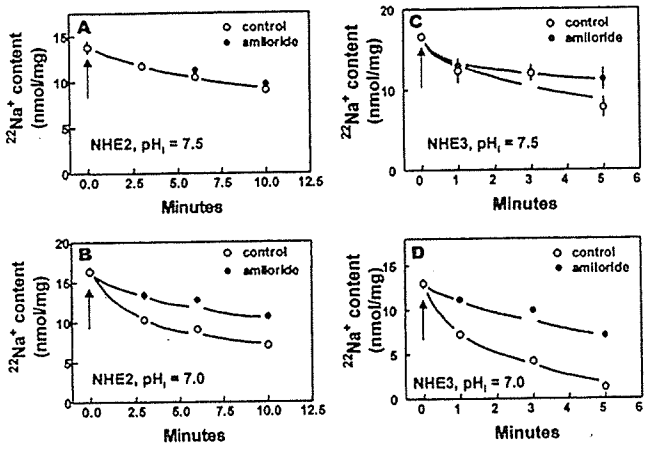

FIG. 5. **Time courses of $^{22}Na^+$ efflux in cells expressing NHE2 or NHE3.** Cells expressing NHE2 or NHE3 were pH$_i$-clamped and $^{22}Na^+$-loaded as described under "Experimental Procedures". *A* and *B*, time courses of $^{22}Na^+$ efflux in cells expressing NHE2 were measured in the absence (○) and presence (●) of 5 mM amiloride at pH$_i$ 7.5 and 7, respectively. *C* and *D*, time courses of $^{22}Na^+$ efflux in cells expressing NHE3 were measured in the absence (○) and presence (●) of 5 mM amiloride at pH$_i$ 7.5 and 7, respectively. Data represent means ± S.D. of three determinations.

DISCUSSION

In this work we tried to kinetically dissect proton-binding sites in the Na^+/H^+ exchanger by measuring EIPA-sensitive $^{22}Na^+$ efflux from cells expressing different NHE isoforms. We loaded cells with $^{22}Na^+$ while clamping pH$_i$ at various values using a K^+/nigericin technique and measured $^{22}Na^+$ efflux at a constant extracellular pH (7.4) in the nominal absence of extracellular Na^+. To avoid possible interaction of cytosolic Na^+ with the H^+ modifier site as suggested previously (14, 25), we limited the extent of $^{22}Na^+$ loading to low levels (2–3 mM). To our knowledge, $^{22}Na^+$ efflux has never been measured using cultured cells under such defined conditions.

$^{22}Na^+$ efflux from cells expressing NHE1, NHE2, or NHE3 was markedly stimulated by cytoplasmic acidification, contrary to the prediction based on reduced H^+ concentration gradient. As proposed previously (9, 10), the results can be interpreted as indicating that these NHE isoforms possess the H^+ modifier site and that occupancy of the latter by a proton(s) results in activation of exchange activity. We observed that the NHE1-mediated $^{22}Na^+$ efflux exhibited roughly bell-shaped pH$_i$ dependence. Modest cytosolic alkalinization (pH$_i$ 7.5) abolished $^{22}Na^+$ efflux (Figs. 1*D*, 2*B*, and 4), whereas modest cytosolic acidification from pH$_i$ 7.5 to 7–7.2 dramatically enhanced it (Figs. 1*C*, 2*B*, and 4). The increase in $^{22}Na^+$ efflux in the latter pH$_i$ range was very steep, suggesting the binding of two or more protons to the modifier site. In a near-neutral pH$_i$ range, cell ATP depletion or mutations of NHE1 (R440D and G455Q) caused marked shifts in the pH$_i$ dependence of $^{22}Na^+$ efflux (Figs. 2*B*, 3*B*, and 4). Because they also caused similar large

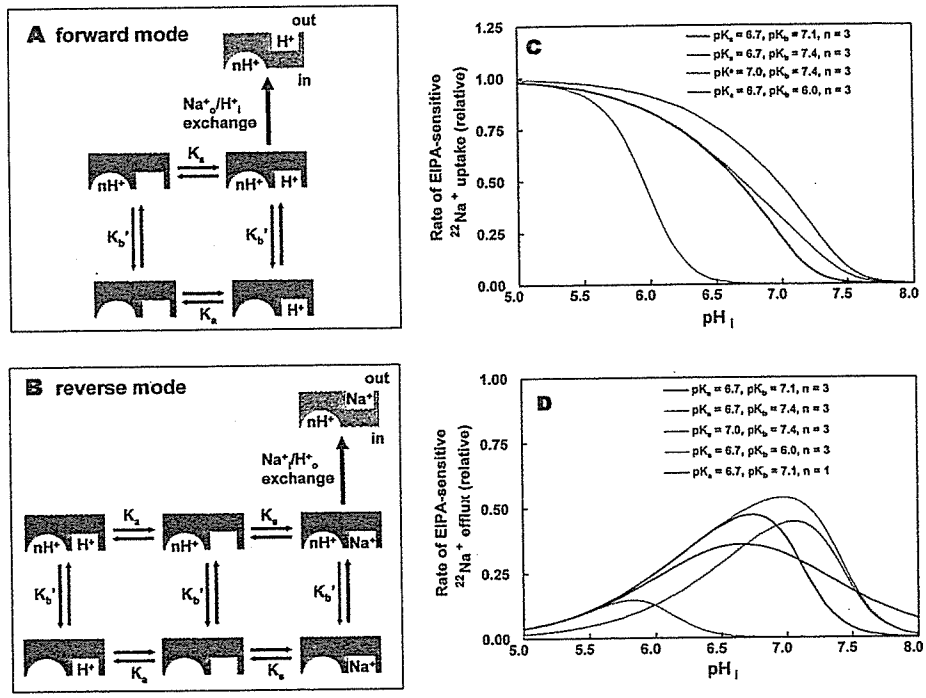

FIG. 6. **Schemes explaining the pH$_i$ dependence of the Na^+/H^+ exchange.** We assumed that multiple protons (*n* molecules) cooperatively bind to the H^+ modifier sites (*circular space*), whereas a single proton binds to the transport site (*rectangular space*) on the cytosolic side of the exchanger. In addition, we assumed that these two types of H^+ binding sites are independent, *i.e.* H^+ binding at one site does not affect the H^+ affinity for the other. In the forward mode of exchange ($^{22}Na^+$ uptake) (*A*), only the exchanger occupied by protons at both sites would be able to participate in the exchange reaction, whereas in the reverse mode of exchange ($^{22}Na^+$ efflux) (*B*), the exchanger having protons at the modifier site but $^{22}Na^+$ at the transport site would become active. In the reverse mode, H^+ would competitively inhibit Na^+ binding at the transport site. Based on these assumptions, we simulated the pH$_i$ dependences of $^{22}Na^+$ uptake (*C*) and $^{22}Na^+$ efflux reactions (*D*). We used the following steady-state equations that were developed assuming a rapid equilibrium of H^+ and Na^+ binding (37): $v/V_{max} = [H^+]/(K_a(1 + (K_b/[H^+])^n) + [H^+](1 + (K_b/[H^+])^n))$ for the relative rate of $^{22}Na^+$ uptake, and $v/V_{max} = [Na^+]/(K_s(1 + [H^+]/K_a + (K_b/[H^+])^n + ([H^+]/K_a)(K_b/[H^+])^n) + [Na^+](1 + (K_b/[H^+])^n)))$ for the relative rate of $^{22}Na^+$ efflux, where K_a and K_b ($K_b' = (K_b)^n$) are the intrinsic H^+ dissociation constants for the transport and modifier sites, respectively, and K_s is the Na^+ dissociation constant for the transport site. For simulation of $^{22}Na^+$ efflux, K_s and the intracellular Na^+ concentration were assumed to be 10 and 2 mM, respectively. The values for other parameters obtained by means of manual fitting trials are given in *panels C* and *D*.

shifts in pH_i dependence of the forward mode of Na^+/H^+ exchange under corresponding conditions (20), it is most likely that modulation of Na^+/H^+ exchange by these procedures is attributable to altered interaction of the H^+ modifier site with activating protons. On the other hand, acidosis ($<pH_i$ 6.2) caused an extensive inhibition of $^{22}Na^+$ efflux (Figs. 2*B* and 4). This inhibition appears to result from competition between Na^+ and H^+ for the intracellular transport site. Our measurement of the descending and ascending slopes of pH_i dependence of $^{22}Na^+$ efflux thus allowed us to observe the binding of protons to the H^+ modifier and H^+ transport sites, respectively. The effect of pH_i on $^{22}Na^+$ efflux from cells was measured previously using thymic lymphocytes (13) in which a significant difference in $^{22}Na^+$ efflux was not observed at the two pH_i values tested (7.2 and 6.3). A possible explanation for such data is that the two pH_i values used for thymic lymphocytes may not be optimal for observing a large pH_i-dependent change in $^{22}Na^+$ efflux.

We attempted to reproduce by simulation the pH_i dependence of the forward and reverse modes of Na^+/H^+ exchange and their modulation by ATP depletion or the exchanger mutations using a simplified reaction model and the assumption that three protons ($n = 3$) cooperatively interact with the modifier site and a single proton interacts with the transport site (Fig. 6, *A* and *B*). We were able to at least qualitatively reproduce complex pH_i profiles of the forward and reverse modes of exchange and their modulation (Fig. 6, *C* and *D*). For example, ATP depletion or mutation of Arg^{440} inhibited the uptake and efflux activities more strongly in the neutral pH_i range (6.6–7.5). In addition, pH_i dependence between 6.6 and 5.6 was very steep when the activity was measured as uptake but not as efflux (Figs. 2 and 4) under ATP depletion or in cells expressing R440D (compare the pH_i profiles in Figs. 2, 4 and 6). Thus our measurement of pH_i dependence of $^{22}Na^+$ efflux permitted us to analyze kinetic properties of the H^+ modifier site interacting with activating protons. The observed properties are compatible with the predicted roles of the exchanger in cell pH_i regulation, *i.e.* protection of cells from excessive alkalosis, acceleration of recovery of cells from acidosis, and modulation of exchange activity due to alteration in H^+ affinity of the modifier site, in particular in the near-neutral pH_i range.

Mutation of Arg^{440} shifts pH_i dependence of the forward mode of Na^+/H^+ exchange toward an acidic side, whereas that of Gly^{455} shifts it toward an alkaline side without changing apparent affinities for extracellular substrates Na^+ and H^+ and the inhibitor EIPA (20) (see Fig. 4*B*). Thus, the present data reinforce our previous conclusion that the region encompassing the intracellular loop IL5 and the transmembrane domain TM11 plays a crucial role in the proper functioning of the H^+ modifier site (20). Although the structure of the H^+ modifier site is not known, we suggested previously that pH_i sensing of NHE1 may be controlled by a substructure consisting of intracellular loop IL5 and the juxtamembrane subdomain I of the cytoplasmic domain (amino acids 503–595) with a tightly bound calcineurin B homologous protein (20, 26). In general, a histidine residue has been thought to be a good candidate for a residue involved in pH_i sensing, because its imidazole moiety is the only side chain that ionizes in solution within a physiological pH range. Indeed, His^{225} and His^{367} have been identified as important residues for pH sensing of the Na^+/H^+ antiporters of *Escherichia coli* (NhaA) (27, 28) and *Schizosaccharomyces pombe* (Sod2) (29, 30), respectively. However, little change was observed in pH_i sensitivity when histidine residues at positions 76, 81, 250, 285, 325, 373, 376, 407, 408, and 473 were substituted by cysteine in NHE1,[2] although a recent study (31) reported that mutations at His^{479} and His^{499} in the juxtamembrane cytoplasmic domain of rabbit NHE3 shifted the pH_i profile to an acidic side. Other histidine residues of NHE1, *i.e.* His^{35}, His^{120} and His^{349} in the membrane-spanning segments (32) and those in the histidine cluster (HYGHHH) in the cytoplasmic domain (30), do not appear to directly influence exchange activity.

Although the present results suggest the existence of a H^+ modifier site in NHEs, it should be noted that complex kinetic effects of protons on exchanger activation have been reported as follows. (i) Transient kinetic studies of the exchanger using kidney brush border membrane vesicles revealed that the exchanger exhibits cooperativity with respect to the external Na^+ concentration when vesicles are acid-loaded (33), suggesting that protonation of the modifier site may change the oligomeric interaction. (ii) Exchange activity of NHE3 (34, 35) or NHE1 (36) is slowly (3~5 min) activated by intracellular acidification, suggesting that a slow conformational change or phosphorylation-dependent event may be involved in the expression of exchanger activity. (iii) Intracellular Na^+ is able to activate the exchanger (14, 25), suggesting a possible interaction of Na^+ with the H^+ modifier site. However, the structural basis for these properties of the H^+ modifier site is not known.

In summary, using cultured cells expressing different NHE isoforms, we obtained evidence for the existence of the H^+ modifier site(s) distinguishable from the H^+ transport site. Our results suggest that interaction of multiple protons with the modifier site results in a dramatic activation of Na^+/H^+ exchange in response to modest acidification. Clearly, further work is required to clarify the structure and function of the H^+ modifier site, which is a hallmark of NHE regulation.

REFERENCES

1. Wakabayashi, S., Shigekawa M., and Pouysségur, J. (1997) *Physiol. Rev.* **77,** 51–74
2. Orlowski, J., and Grinstein, S. (1997) *J. Biol. Chem.* **272,** 22373–22376
3. Counillon, L., and Pouysségur, J. (2000) *J. Biol. Chem.* **275,** 1–4
4. Grinstein, S., Rotin, D., and Mason, M. J. (1989) *Biochim. Biophys. Acta* **988,** 73–97
5. Moolenaar, W. H., Tsien, R. Y., van der Saag, P. T., and de Laat, S. W. (1983) *Nature* **304,** 645–648
6. Paris, S., and Pouysségur, J. (1984) *J. Biol. Chem.* **259,** 10989–10994
7. Grinstein, S., Rothstein, A., and Cohen, S. (1985) *J. Gen. Physiol.* **85,** 765–787
8. Wakabayashi, S., Bertrand, B., Ikeda, T., Pouysségur, J., and Shigekawa, M. (1994) *J. Biol. Chem.* **269,** 13710–13715
9. Aronson, P. S., Nee, J., and Suhm, M. A. (1982) *Nature* **299,** 161–163
10. Aronson, P. S. (1985) *Ann. Rev. Physiol.* **47,** 545–560
11. Vigne, P., Frelin, C., and Lazdunski, M. (1984) *EMBO J.* **3,** 1865–1870
12. Grinstein, S., Cohen, S., and Rothstein, A. (1984) *J. Gen. Physiol.* **83,** 341–369
13. Grinstein, S., Goetz, J. D., and Rothstein, A. (1984) *J. Gen. Physiol.* **84,** 585–600
14. Green, J., Yamaguchi, D. T., Kleeman, C. R., and Muallem, S. (1988) *J. Gen. Physiol.* **92,** 239–261
15. Vaughan-Jones, R. D., and Wu, M.-L. (1990) *J. Physiol.* **428,** 441–466
16. Wakabayashi, S., Fafournoux, P., Sardet, C., and Pouysségur, J. (1992) *Proc. Natl. Acad. Sci. U. S. A.* **89,** 2424–2428
17. Tse, C.-M., Levine, S. A., Yun, C. H., Brant, S. R., Pouysségur, J., Montrose, M. H., and Donowitz, M. (1993) *Proc. Natl. Acad. Sci. U. S. A.* **90,** 9110–9114
18. Orlowski, J. (1993) *J. Biol. Chem.* **268,** 16369–16377
19. Pouysségur, J., Sardet, C., Franchi, A., L'Allemain, G., and Paris, S. (1984) *Proc. Natl. Acad. Sci. U. S. A.* **81,** 4833–4837
20. Wakabayashi, S., Hisamitsu, T., Pang, T., and Shigekawa, M. (2003) *J. Biol. Chem.* **278,** 11828–11835
21. Ikeda, T., Schmitt, B., Pouysségur, J., Wakabayashi, S., and Shigekawa, M. (1997) *J. Biochem. (Tokyo)* **121,** 295–303
22. Cassel, D., Katz, M., and Rotman, M. (1986) *J. Biol. Chem.* **261,** 5460–5466
23. Goss, G. G., Woodside, M., Wakabayashi, S., Pouysségur, J., Waddell, T., Downey, G. P., and Grinstein, S. (1994) *J. Biol. Chem.* **269,** 8741–8748
24. Deleted in proof
25. Green, J., Yamaguchi, D. T., Kleeman, C. R., and Muallem, S. (1988) *J. Biol. Chem.* **263,** 5012–5015
26. Pang, T., Su, X., Wakabayashi, S., and Shigekawa, M. (2001) *J. Biol. Chem.*

[2] S. Wakabayashi, T. Hisamitsu, T. Pang, and M. Shigekawa, unpublished observations.

276, 17367–17372
27. Gerchman, Y., Olami, Y., Rimon, A., Taglicht, D., Schuldiner, S., and Padan, E. (1993) *Proc. Natl. Acad. Sci. U. S. A.* **90,** 1212–1216
28. Rimon, A., Gerchman, Y., Olami, Y., Schuldiner, S., and Padan, E. (1995) *J. Biol. Chem.* **270,** 26813–26817
29. Dibrov, P., Young, P. G., and Fliegel, L. (1998) *Biochemistry* **37,** 8282–8288
30. Wiebe, C. A., Dibattista, E. R., and Fliegel, L. (2001) *Biochem. J.* **357,** 1–10
31. Cha, B., Oh, S., Shanmugaratnam, J., Donowitz, M., and Yun, C. C. (2003) *J. Membr. Biol.* **191,** 49–58
32. Wang, D., Balkovetz, D. F., and Warnock, D. G. (1995) *Am. J. Physiol.* **269,** C392–C402
33. Otsu, K., Kinsella, J. L., Heller, P., and Froehlich, J. P. (1993) *J. Biol. Chem.* **268,** 3184–3193
34. Kinsella, J. L., Heller, P., and Froehlich, J. P. (1998) *Biochem. Cell Biol.* **76,** 743–749
35. Hayashi, H., Szászi, K., Coady-Osberg, N., Orlowski, J., Kinsella, J. L., and Grinstein, S. (2002) *J. Biol. Chem.* **277,** 11090–11096
36. Haworth, R. S., McCann, C., Snabaitis, A. K., Roberts, N. A., and Avkiran, M. (2003) *J. Biol. Chem.* **278,** 31676–31684
37. Segel, I. V. (1975) *Enzyme Kinetics: Behavior and Analysis of Rapid Equilibrium and Steady-state Enzyme Systems*, pp. 346–464, John Wiley & Sons, Inc., New York

Journal of Cerebral Blood Flow & Metabolism
23:395–398 © 2003 The International Society for Cerebral Blood Flow and Metabolism
Published by Lippincott Williams & Wilkins, Inc., Philadelphia

Short Communication

Cyclooxygenase-2 Expression Associated With Spreading Depression in a Primate Model

*Chiaki Yokota, †Hiroyasu Inoue, ‡Yuji Kuge, §Takeo Abumiya, ‖Masafumi Tagaya, ¶Yasuhiro Hasegawa, #Norimasa Ejima, **Nagara Tamaki, and ¶Kazuo Minematsu

**Cerebrovascular Laboratory, Department of Pathogenesis, and †Department of Pharmacology, National Cardiovascular Center Research Institute, Departments of ‡Tracer Kinetics and **Nuclear Medicine, Graduate School of Medicine, Hokkaido University §Department of Neurosurgery, Ebetu Hospital, ‖Department of Medicine, National Osaka Hospital, ¶Cerebrovascular Division, Department of Medicine, National Cardiovascular Center, and #Institute for Biofunctional Research Co., Inc., Osaka, Japan*

Summary: The authors previously provided evidence that spreading depression (SD) can be evoked in primates. Cyclooxygenase-2 (COX-2) expression has been found to increase in the rodent cortex undergoing SD, and the authors sought to determine whether this association exists in primate brain. In the present study, neuronal COX-2 expression was induced during SD in the primate cortex. The mean expression ratio of COX-2 messenger RNA in animals with SD was significantly higher than that measured in controls (1.69 vs. 0.5; $P = 0.02$). Induction of COX-2 in these animals was also detected by human microarray analysis. Results show that, as in rodents, neuronal COX-2 is induced in the primate cortex in response to SD. **Key Words:** Spreading depression—Cyclooxygenase-2—Microarray analysis—Primate.

Cortical spreading depression (SD), the reversible depression of cortical electrical activity, plays a role in the development of cerebral ischemic injury and migraine (Lauritzen et al., 1983; Olesen et al., 1981; Woods et al., 1994). Repetitive, pathologic SDs were similarly found to play a role in the development of ischemic injury under conditions of focal brain ischemia in rats (Gill et al., 1992; Hossmann, 1994; Iijima et al., 1992; Takano et al., 1996). Changes in cerebral blood flow (CBF) in experimental SD models in rats and cats were characterized by transient focal cortical hyperemia, followed by persistent hypoperfusion (Kuge et al., 2000; Lauritzen et al., 1982; Piper et al., 1991). Recently, we provided the first direct evidence that SD, accompanied by focal cortical hyperemia, can be evoked in primates (Yokota et al., 2002). The long-lasting hypoperfusion that followed this hyperemia in rats and cats has not been observed in primates.

The gene for cyclooxygenase-2 (COX-2), a rate-limiting enzyme in prostaglandin synthesis, was induced in the nonprimate cortex during SD (Koistinaho et al., 1999; Miettinen et al., 1997). Cyclooxygenase-2 appeared to mediate the increase in CBF produced by synaptic activity in the somatosensory cortex in mice (Niwa et al., 2000). The contribution of SD and its associated genes to the pathogenesis of human brain diseases has not been elucidated.

As a first step in determining which genes show altered expression during SD in primates, we examined whether the COX-2 gene was upregulated. Using a human complementary DNA (cDNA) array system, we also examined the effect of SDs on gene-expression profiles.

MATERIALS AND METHODS

Spreading depression model and brain preparation

Nine adult, male cynomolgus monkeys were divided into two groups: a normal control group (group C, n = 3) and a group in which SD was evoked by applying 3.3-mol/L KCl to

Received September 18, 2002; final version received December 9, 2002; accepted December 9, 2002.

This study was supported in part by Special Coordination Funds for Promoting Science and Technology (Strategic Promotion System for Brain Science) from the Ministry of Education, Culture, Sports, Science and Technology of Japan, by a Grant-in-Aid for Scientific Research from the Japan Society for the Promotion of Science, by a grant from the Takeda Medical Research Foundation in Japan, and by a Japan Heart Foundation Research Grant.

Address correspondence and requests to Dr. Yokota, Cerebrovascular Laboratory, National Cardiovascular Center Research Institute, 5-7-1 Fujishirodai, Suita, Osaka 565-8565, Japan; e-mail: cyokota@ri.ncvc.go.jp

DOI: 10.1097/01.WCB.0000055293.67563.2E

the cortex (group SD, n = 6). All procedures were approved by our Institutional Animal Research Committee and were performed in accordance with standards published by the National Research Council in the *Guide for the Care and Use of Laboratory Animals*.

Shifts of direct current potential were measured in four animals in the SD group only with a microelectrode placed just rostral to the chemical stimulation site; a single episode was recorded in three animals, and six episodes were recorded in one animal. Direct current potential was measured in the remaining two animals with a microelectrode that was placed caudal to the chemical stimulation site as well as with microelectrodes placed rostral to the chemical stimulation site; one of these animals was subjected to eight recording episodes at this site, whereas the remaining animal was subjected to two direct current shifts, each of which was recorded from a point that was rostrally adjacent to the chemical stimulation site, as well as to six episodes at the caudal site.

Two hours after KCl application, the brains from these animals were perfused with cold saline, after which the animals were killed and the brains removed. Several samples from each cortex were harvested and stored at −80°C until use, whereas other samples were embedded in paraffin.

RNA blot analysis

RNA preparation and blot analysis were performed as previously described (Inoue et al., 1995). Cyclooxygenase-2 messenger RNA (mRNA) in each region was expressed as the ratio of the COX-2 mRNA signal to the GAPDH mRNA signal in that region (expression ratio).

Microarray analysis

Microarray analysis was conducted using Genome System (St. Louis, MO, U.S.A.) as described elsewhere (Lyer et al., 1999). The microarray contained 9,182 elements: 8,412 unique annotated genes or expressed sequence tags, and 4,757 characterized human protein genes. Left cortical RNAs from the SD (>5 episodes; n = 3) and control (n = 3) groups were pooled. Poly $(A)^+$ RNAs were purified from these RNAs using oligo$(dT)_{30}$-latex (Takara, Inc., Shiga, Japan) to use as templates for cDNA synthesis. The cDNA probes were reverse transcribed with 5′Cy3 or fluorescently labeled Cy5 and were hybridized with Human UniGEM V (version 2.0). The average of the total Cy3 and Cy5 signals yielded a ratio that was used to normalize the signals.

Immunoblot analyses

Left temporal cortical samples were weighed and homogenized in 10 volumes of cold 62.5-mmol/L Tris buffer (pH 6.8) containing 1% sodium dodecylsulfate, 10% glycerin, and 5% 2-mercaptoethanol. Tissue homogenates were heated to 90°C for 5 minutes and then centrifuged at 15,000*g* for 10 minutes at 4°C. The supernatants were separated by SDS-PAGE (5% to 20% acrylamide gradient) and proteins transferred onto a nitrocellulose sheet. The blots were incubated with anti–COX-2 antibody (dilution 1:1,000; Cayman Chemical, Ann Arbor, MI, U.S.A.) for 1 h at 25°C and were then washed in 50-mmol/L phosphate-buffered saline (pH 7.4) containing 0.05% Tween 20.

Immunohistochemistry

A mirror-sectioning technique was used to colocalize COX-2 and microtubule-associated protein 2 (MAP-2), a neuronal skeletal protein. Deparaffinized temporal cortical sections (3 μm) were incubated with a polyclonal anti–COX-2 antibody (dilution 1:100; Cayman Chemical) and a monoclonal anti–MAP-2 antibody (clone HM-2; dilution 1:2,400; Sigma, St. Louis, MO, U.S.A.) overnight at 4°C. The sections were washed with phosphate-buffered saline, and biotinylated goat anti–rabbit immunoglobulin (Vector Laboratories, Burlingame, CA, U.S.A.) or biotinylated $F(ab')_2$ rabbit anti–mouse immunoglobulin (dilution 1:500; Dako, Carpinteria, CA, U.S.A.) was applied to the sections, which were then incubated for 30 minutes at 25°C. Labeling was visualized using a Vectastain Elite Kit (Vector Laboratories).

Statistical analysis

Data are expressed as the mean ± standard deviation. Comparisons of COX-2 mRNA expression between groups were made using the Mann-Whitney *U* test. A two-tailed *P* value less than 0.05 was considered to be significant.

RESULTS

Expression of cyclooxygenase-2 mRNA

Cyclooxygenase-2 mRNA expression increased in the cortex in which SD was induced (left) compared with both the contralateral side and the left cortex in group C (Fig. 1A). The expression ratio of COX-2 mRNA in the left cortex in the SD group (1.69 ± 0.57) was significantly greater ($P = 0.02$) than in the left cortex in group C (0.5 ± 0.05; Fig. 1B).

Cyclooxygenase-2 localization

Immunoblots revealed a 70- to 72-kd COX-2–immunoreactive band (Gidlund et al., 1981) in tissue derived from the SD group, which was barely detectable in group C (Fig. 1C). Immunoreactive neurons were observed in animals that received six SD episodes rostral to the chemical stimulation site (Fig. 1D). Immunoreactive MAP-2 was demonstrable in the same neurons that displayed COX-2 immunoreactivity.

Gene-expression patterns

Increases in normalized gene-expression signals above 1.5-fold were observed for two genes among a total 9,182 elements: the COX-2 (1.6-fold) and basic transcription element–binding protein 1 (1.6-fold) genes. Twenty-one elements were found to be different by at least 1.4-fold. Figure 2 shows representative images of scanned arrays hybridized with left cortical samples.

DISCUSSION

Previous studies have suggested that COX-2 plays a role in the development of ischemic injury during focal brain ischemia in rodents (Collaco-Moraes et al., 1996;

FIG. 2. Gene-expression patterns in the brains of animals in the spreading depression (SD) and control (C) groups. Representative images of scanned arrays hybridized with cortical samples from C and SD animals are shown. Of the 9,182 elements that were examined, expression of the cyclooxygenase-2 gene (red circles) was found to be increased by 1.6-fold in the SD group.